Contents lists available at ScienceDirect

Petroleum Science

journal homepage: www.keaipublishing.com/en/journals/petroleum-science



Original Paper

Numerical simulation of rock-breaking and influence laws of dynamic load parameters during axial-torsional coupled impact drilling with a single PDC cutter



Yan Xi a, Hao-Yu Wang a, Chun-Qing Zha a, Jun Li b, c, Gong-Hui Liu a, Bo-Yun Guo d

- ^a Beijing University of Technology, Beijing, 100124, China
- ^b China University of Petroleum-Beijing, Beijing, 102249, China
- ^c China University of Petroleum-Beijing at Karamay, Karamay, Xinjiang, 834000, China
- ^d University of Louisiana at Lafayette, Lafayette, 70504, USA

ARTICLE INFO

Article history: Received 28 July 2022 Received in revised form 16 November 2022 Accepted 11 January 2023 Available online 13 January 2023

Edited by Jia-Jia Fei

Kevwords: Axial-torsional coupled impact drilling tool Rock-breaking PDC cutter RHT model

ABSTRACT

Axial and torsional impact drilling technology is used to improve the drilling efficiency of hard rock formation in the deep underground. Still, the corresponding theory is not mature, and there are few correlative research reports on the rock-breaking mechanism of axial and torsional coupled impact drilling tools. Considering the influence of the impact hammer geometry and movement on the dynamic load parameters (i.e., wavelength, amplitude, frequency, and phase difference), a numerical model that includes a hard formation and single polycrystalline diamond compact cutter was established. The Riedel-Hiermaier-Thoma model, which considers the dynamic damage and strength behavior of rocks, was adopted to analyze the rock damage under axial and torsional impact loads. The numerical simulation results were verified by the experimental results. It was found that compared with conventional drilling, the penetration depths of axial, torsional, and axial-torsional coupled impact drilling increased by 31.3%, 5.6%, and 34.7%, respectively. Increasing the wavelength and amplitude of the axial impact stress wave improved the penetration depth. When the bit rotation speed remained unchanged, increasing the frequency in the axial and circumferential directions had little effect on the penetration depth. However, as the frequency increased, the cutting surface became increasingly smooth, which reduced the occurrence of bit vibration. When the phase difference between the axial and circumferential stress waves was 25%, the penetration depth significantly increased. In addition, the bit vibration problem can be effectively reduced. Finally, the adjustment of engineering and tool structure parameters is proposed to optimize the efficiency of the axial-torsional coupled impact drilling tool.

© 2023 The Authors. Publishing services by Elsevier B.V. on behalf of KeAi Communications Co. Ltd. This is an open access article under the CC BY-NC-ND license (http://creativecommons.org/licenses/by-nc-nd/

4.0/).

1. Introduction

The continuous exploration and development of deep and ultradeep reservoirs have focused the attention of engineers and researchers on the improvement of drilling efficiency (Singh et al., 2009; Li and Wang, 2015; Ji et al., 2020; Liao et al., 2021). It was prompted by the increase in the true vertical depth of oil and gas wells, which has increased the hardness, compressive strength, abrasiveness, and other mechanical parameters that reduce the drillability of rocks (Wang et al., 2021; Xi et al., 2021). Reduced

drillability could decrease the rate of penetration (ROP), increase drill teeth wear, and reduce the service life of drill bits, all of which increase the investment costs of the drilling process (Shi et al., 2015; Wu and Ye, 2019). Technologies for improving the ROP have been proposed, including impact drilling, hydraulic oscillators, and hydraulic pulsed cavitating jet-assisted drilling (Liu et al., 2019; Mu et al., 2020; Wang et al., 2021). Among these, impact drilling has been extensively applied in deep wells in various blocks, and has been found to enhance the ROP by approximately 30%-50% (Staysko et al., 2011; Li et al., 2020; Song et al., 2021). Rotary and torsional impact drilling tools have been designed based on this technology. A rotary impact drilling tool can be employed to apply an additional impact load in the axial direction to enhance the

E-mail address: xiyan@bjut.edu.cn (Y. Xi).

^{*} Corresponding author.

penetration depth of the drill bit. Torsional impact drilling tools apply an impact load in the circumferential direction, which improves the efficiency of traditional rock cutting and reduces stickslip vibration (Franca, 2011; Saksala et al., 2014; Wang et al., 2018; Zhang et al., 2019; Xi et al., 2021). In recent years, researchers have attempted to combine these two impact drilling technologies to exploit their rock-breaking advantages. As a result, various types of axial-torsional coupled impact drilling tools have been proposed and developed (Xu et al., 2016; Zha et al., 2017; Liu et al., 2018; Wang et al., 2021). Because such technology and tools are new, research on the corresponding rock-breaking mechanisms remains insufficient, limiting their further development. Therefore, it is necessary to perform related research.

The axial-torsional coupled impact drilling tool, also known as a compound percussive/impact drilling tool or multi-dimensional impactor, has been studied by many engineers and scholars (Liu et al., 2016, 2018; Mu et al., 2020; Wang et al., 2021; Li et al., 2020, 2021). Some have investigated the rock-breaking mechanism of the axial-torsional coupled impact drilling tool by theoretical analysis and numerical simulation methods. Others have carried out field engineering tests to analyze the effects of the increased ROP caused by the new device. Liu et al. (2016) found that compound percussive drilling technology could be used to conduct three-dimensional rock breaking to improve the ROP and wellbore quality. Liu et al. (2018) studied the impact of the inclination angle of the drill teeth during compound impact drilling. They found that the maximum volume of broken rock was obtained at an inclination angle of 50°. Liu et al. (2020) designed a multi-dimensional impactor, i.e., an axial-torsional coupled impact drilling tool. Their field tests showed that the ROP of the multi-dimensional impactor was 7.1%-98.5% higher than that of conventional drilling. Mu et al. (2020) proposed an axial-torsional coupled percussion drilling tool and applied it to a drilling field. Their results showed that the ROP increased by at least 60%. Wang et al. (2021) and Li et al. (2021) analyzed the law of crack generation for rockbreaking during compound impact drilling. However, the effects of different parameters on the penetration depth and rock-breaking volume were not considered. In these studies, the impact parameters of the axial-torsional coupled impact drilling tool, such as the wavelength, amplitude, frequency, and phase difference, were rarely considered. Therefore, it is essential to conduct relevant research to improve the performance of the axial-torsional coupled impact drilling tool.

Scholars have demonstrated the influence of impact parameters on the rock-breaking effect through laboratory tests and numerical simulations (Xi et al., 2021). Xi et al. (2021) analyzed the impact parameters of a rotary impact drilling tool for rock breaking. Their results showed that increasing the amplitude and changing the waveform enhanced the penetration depth and rock-breaking volume. The impact parameters are also the basis for optimizing the geometric parameters of the core assembly of the axialtorsional coupled impact drilling tool. This can be explained as follows. First, during the movement of the internal components of the coupled impact drilling tool, the impact hammers (e.g., axial and torsional impact hammers) generate a stress wave during the impact process. The geometric (length and shape) and movement parameters (impact velocity) of the impact hammer directly influence the parameters of the generated stress wave (amplitude, frequency, action time, and waveform). As a result, the relationship between the parameters of the impact hammers and stress wave should be established. Second, as the generated stress wave spreads into the rock along the direction of the bit-rock interface, it damages the rock near the impact area, which improves the rockbreaking efficiency. Different waves cause different types of rock damage, directly affecting the penetration depth of the drill teeth and the size of the rock cuttings after rock breaking. Parameter optimization (e.g., impact amplitude, frequency, and waveform) results in the best rock-breaking effect for specific hard formations. Thus, the relationship between the stress wave parameters and the rock-breaking effect must be established. Some researchers have conducted preliminary theoretical research and laboratory tests that confirmed the influence of the geometric and motion parameters of the hammer on the waveform. However, relevant studies on optimizing the mechanical structural parameters of the axialtorsional coupled impact drilling tool remain few.

The lack of relevant research is attributed to three main factors. The first is the complexity of the load applied to the drill bit during the axial-torsional coupled impact drilling process. Before using the impact drilling tool, the axial static load transmitted from the drill string to the drill bit acts on the rock. The continuous rotation of the drill bit causes a displacement load and shearing of the rock. After the impact drilling tool is applied, axial and tangential shock waves are generated and transmitted to the drill bit, which improves the rock-breaking effect. The complex mechanical environment of the drill bit makes the performance of relevant theoretical analyses and experimental research a challenge. Second, the dynamic characteristics of the rock must be considered during the axial-torsional coupled impact drilling process. The stroke of the axial hammer is always 400 mm, and the frequency can reach 40 Hz, while the impact frequency of the torsional impact hammer can exceed 60 Hz

Table 1 Parameter description of the RHT material model.

Parameter	Symbol	Value	Parameter	Symbol	Value
Mass density, kg/m ³	ρ_0	2680	Lode angle dependence factor	Q_0	0.63
Initial porosity	α_0	1.1	Lode angle dependence factor	В	0.0105
Crush pressure, MPa	p_{el}	0.04	Porosity exponent	N	4
Compaction pressure, GPa	$p_{\rm comp}$	0.54	Reference compressive strain-rate	ε_0^{c}	3.0e-8
Hugoniot polynomial coefficient, GPa	A_1	76.48	Reference tensile strain rate	$\varepsilon_0^{\mathrm{t}}$	3.0e-9
Hugoniot polynomial coefficient, GPa	A_2	128.48	Break compressive strain rate	ε^{c}	3.0e22
Hugoniot polynomial coefficient, GPa	A_3	78.53	Break tensile strain rate	ε^{t}	3.0e22
Parameter for polynomial EOS	B_0	1.68	Compressive strain rate dependence exponent	β_{c}	0.0106
Parameter for polynomial EOS	B_1	1.68	Tensile strain rate dependence exponent	β_{t}	0.0144
Parameter for polynomial EOS, GPa	T_1	76.48	Compressive yield surface parameter	g_{c}'	0.42
Parameter for polynomial EOS	T_2	0	Tensile yield surface parameter	g_{t}'	0.7
Elastic shear modulus, GPa	G	19.40	Shear modulus reduction factor	ξ	0.48
Compressive strength, MPa	$f_{\rm c}$	0.118	Damage parameter	D_1	0.042
Relative tensile strength	$f_{ m t}{}'$	0.11	Damage parameter	D_2	1
Relative shear strength	$f_{s}{}'$	0.37	Minimum damaged residual strain	$\varepsilon_{\mathrm{p}}^{\mathrm{m}}$	0.012
Failure surface parameter	Α	1.59	Residual surface parameter	$\hat{A_{ m f}}$	1.63
Failure surface parameter	n	0.58	Residual surface parameter	$n_{ m f}$	0.6

(Li et al., 2021). The axial and torsional impact hammers' maximum impact speeds exceed 6 m/s. Under these conditions, the rockbreaking process belongs to the category of rock dynamics. Therefore, the dynamic characteristics of rocks must be considered during the analysis. Xi et al. (2021, 2022) simulated the rockbreaking process during impact drilling, considering the rock dynamic characteristic parameters. The simulated results corresponded with the experimental results, and proved that the Riedel-Hiermaier-Thoma (RHT) material model accurately reflects the rock-breaking process of the impact drilling tool. Third, the rockbreaking mechanism under the condition of shockwave coupling in different directions is highly complex. Some scholars have only studied the influence of the stress wave parameters in one direction (axial or circumferential) on rock-breaking efficiency (Song et al., 2019; Xi et al., 2021). There are deficiencies in the analysis of stress waves in two directions that act simultaneously. When two stress waves exist simultaneously in different directions, the compatibility between the wavelength, amplitude, and frequency of the two stress waves, and the phase differences of the two stress waves influence the rock-breaking effect. As a result, further studies are required on the rock-breaking mechanisms of the axialtorsional coupled impact drilling tool.

In this study, the differences in axial-torsional coupled impact drilling tool structures are considered, and the relationship between the geometric and motion parameters of the impact hammer and the wave parameters is established. The RHT model, which considers the dynamic rock characteristics, is used to analyze the rock damage under axial and torsional impact loads. A numerical model is established to investigate the rock-breaking process of the bit cutter, and a series of numerical simulations are performed. The penetration depth and rock-breaking process of different drilling methods (i.e., conventional, rotary impact, torsional impact, and axial-torsional coupled impact drilling) are compared. The sensitivity parameters of axial-torsional coupled impact drilling (i.e., action time, amplitude, frequency, and phase difference) are analyzed. Suggestions for optimizing the structural parameters of the axial-torsional coupled impact drilling tool are provided.

2. Analysis of factors influencing stress wave parameters

The relationship between the geometric and motion parameters of the impact hammers and the shock wave parameters, and that between the shock wave parameters and rock-breaking effects must be established. Split-Hopkinson pressure bar (SHPB) experiments and numerical simulations were conducted to establish the relationship between the hammer geometry, motion parameters, and shock wave parameters. Then, numerical simulations based on rock dynamics were conducted to establish the relationship between the shock wave parameters and rock-breaking effects (i.e., penetration depth, eroded rock volume, and cutting size), considering the ROP and borehole cleanliness. Finally, suggestions for optimizing the structural and kinematic parameters of the impact hammers are presented (see Fig. 1).

2.1. Comparison of different types of impact hammers

There are various types of axial-torsional coupled impact drilling tools (Mu et al., 2020; Wang et al., 2021; Li et al., 2021). To analyze the motion of these tools, one tool was selected for analysis, as shown in Fig. 2. The tool was connected below the drill collar and above the drill bit. During the drilling process, the drilling fluid flows into the impact drilling tool from the drill pipe at a certain flow rate and pressure, and then drives the axial impact hammer to move back and forth in the axial direction and rotate back and forth in the circumferential direction. This process transforms fluid

energy into mechanical energy. The generated stress wave passes through the drill bit and acts on the rock to play an auxiliary role in rock breaking.

Fig. 2 shows that both the axial and torsional impact hammers are annular, with the torsional impact hammer significantly longer than the axial impact hammer. Fig. 3 shows the different types of axial-torsional coupled impact drilling tool structures. The differences between the tools can be explained as follows. For the first tool shown in Fig. 3a, the axial and torsional impact hammers are annular, with the torsional impact hammer significantly longer than the axial impact hammer. For the second tool shown in Fig. 3b, the axial impact hammer is an approximate cylinder; both ends have a large diameter, the middle has a small diameter, and the torsional hammer has an annular shape. There are significant differences between the shape of the impact hammers of the axial-torsional coupled impact drilling tools with different structures. The length and geometry of the hammer (annular and cylindrical) directly influence the rock-breaking effect.

The torsional impact hammer is mainly annular because of its movement mode and tool structure; however, its length and thickness differ. The axial impact hammer can be cylindrical or annular, with a significant difference in shape or size. These differences affect the rock-breaking and stress wave parameters generated during the hammer impact process.

2.2. Experiments of SHPB

2.2.1. Experimental device of SHPB

The Split-Hopkinson Pressure Bar (SHPB) experimental device has been extensively applied to measure the stress waveform and dynamic rock parameters of different materials (Fan et al., 2017, 2018). According to Fig. 4, the equipment consists of five main parts: the dynamic impact loading device, speed test device, video capture device, waveform collection device, and bar system. The bar system comprises striker, incident, and transmission bars, all of which are rigid bodies with an elastic modulus of 210 GPa. The diameters of all the bars were 50 mm, and the lengths of the striker, incident, and transmission bars were 400 mm, 2500 mm, and 2500 mm, respectively.

The SHPB experimental device can be used to simulate the working state of the impact drilling tool in a well. The similarities between the two are as follows. The striker bar can be used to characterize the impact hammer, generating the stress wave in the impact process; the incident bar can be used to represent the drilling tool, which is below the hammer and above the bit. The generated shock wave passes through this section and acts on the rock. Rock samples were used to characterize the impacted hard formations.

2.2.2. SHPB test results

During the experiment, two types of striker bars, used to represent the impact hammers, were selected to establish the relationship between the striker bars and the waveform. The first type of striker bar has a cylindrical shape with a length and diameter of 600 mm and 50 mm, respectively; the second type is in the shape of a spindle with a length of 400 mm. The diameters of both ends are 40 mm and 20 mm, respectively, while the diameter of the middle is 50 mm.

Fig. 5 shows the waveforms produced by the striker bars of different shapes. The differences in stress waves under different conditions were mainly reflected in the following three aspects. First, there were significant differences in the waveforms, which were primarily affected by the hammer geometry. When a cylindrical striker bar was used, the shock wave generated was rectangular; when a spindle striker bar was used, a sine wave was

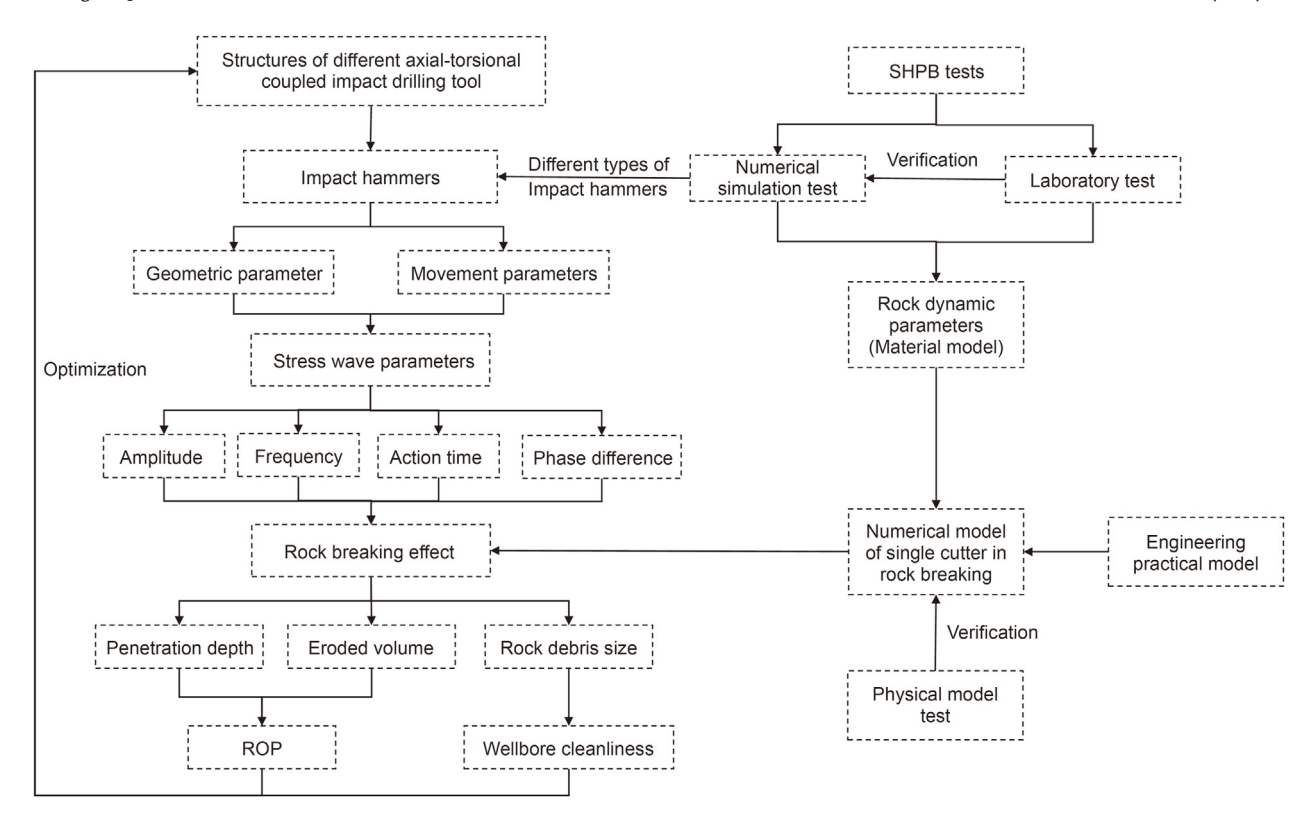


Fig. 1. Flowchart of using the rock dynamics method to optimize the impact tool.

generated. Second, the amplitudes of the rectangular and sine waves were different. At the same impact speed, the difference in the peak load was attributed to the different weights of the two types of hammers (Li et al., 2011). The greater the hammer weight, the greater the amplitude. Third, the wavelengths of the two types of waves were different and mainly determined by the length of the hammer. The longer the hammer, the longer the waveform.

Based on these tests, it can be observed that the geometric parameters and weight of the hammer are closely related to the generated waveform. By changing the relevant parameters of the hammer, the parameters of the shock wave can be adjusted and optimized.

2.3. Relationship between waveform parameters and hammer parameters

2.3.1. Numerical simulation of SHPB

The SHPB test confirmed significant differences in the shock wave shapes generated by different hammer shapes. However, owing to limitations in the geometric size and test equipment performance, it is difficult to test an impact hammer that is roughly similar to that of the impact drilling tool; the consideration of the impact speed is also limited. As a result, a series of SHPB numerical models were established, as shown in Fig. 6. Three cases were considered.

a) The geometry of the axial impact hammer is cylindrical. The impact hammer of some axial-torsional coupled impact drilling tools is approximately cylindrical, as shown in Fig. 3a. The length and diameter of the hammer are 600 mm and 50 mm, respectively. To analyze the influence of the impact hammer shape on the waveform, the hammer is divided into two parts. The diameter of the first half of the hammer was maintained, while that of the second half was changed, as shown in Fig. 6a.

- b) The geometry of the axial impact hammer is considered to be an annulus, and the geometric model mainly considers that the shape of part of the axial hammer is annular, as shown in Fig. 3b. The inner and outer diameters of the hammer were initially set as 178 mm and 138 mm, respectively. Then, one parameter was maintained, while another parameter was changed to analyze the influence of the shape change of the annular hammer on the stress wave parameters.
- c) In all numerical models, the influence of velocity variations on the stress wave waveform is also taken into account. In the numerical simulation, the impact hammer hits the incident bar at a specific initial velocity to generate a shock wave that passes through the rock to the transmission bar. The impact velocity could be adjusted by changing the pressure of the drilling fluid. Previous studies have shown that the impact velocity of the hammer is often directly proportional to the fluid pressure.

2.3.2. SHPB simulation results

When the impact hammer is cylindrical, the shape of the incident wave is rectangular, as shown in Fig. 7a. As the impact velocity increased, the shape of the stress wave remained unchanged while the amplitude increased. This indicates that increasing the shock velocity increases the wave amplitude.

The impact speed was kept unchanged, the shape of the hammer was changed, and the diameter of one end continuously decreased. With decreasing diameter, the shape of the stress wave changed from rectangular to triangular and then to a sine wave, while the amplitude decreased, as shown in Fig. 7b. This was attributed to the change in hammer geometry, which reduced the hammer's weight, resulting in a decrease in amplitude and a change in the waveform.

When the hammer has an annulus shape, the shape of the incident wave is approximately rectangular with a noticeable

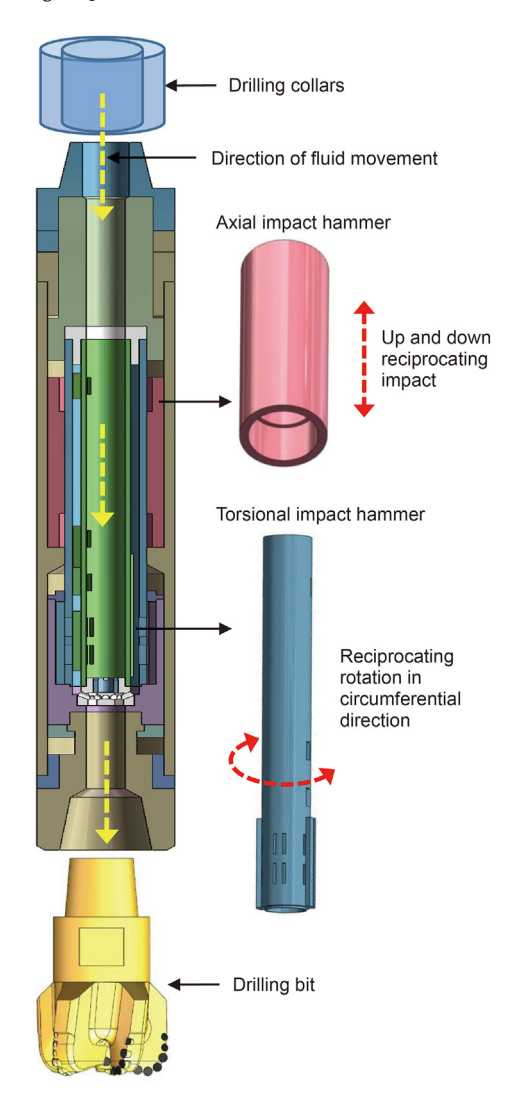


Fig. 2. The axial-torsional coupled impact drilling tool structure.

fluctuation at the peak position, as shown in Fig. 8a, b (OD and ID represent outer diameter and inner diameter, respectively). When the impact velocity is unchanged, changing the inner or outer diameter of the hammer has little effect on the waveform. Only the peak value of the incident wave is affected, primarily because changes in the inner and outer diameters affect the hammer's weight. Under the same conditions, the greater the hammer weight, the higher the amplitude.

3. Numerical simulation

3.1. Engineering model

In the drilling process, the polycrystalline diamond compact (PDC) bit invades the rock through the axial and circumferential loads. To further simplify the calculation model, a single tooth on the bit was selected for analysis (Fig. 9a). The drill bit rotates continuously along the centerline of the drill string during the drilling process; hence, a rotating PDC cutter at a certain time was selected in this study (Fig. 9b). At this time, the PDC cutter receives the load from the axial and tangential directions. The bottom of the centerline of the drill teeth intrudes into the rock at the most significant depth; hence, the change in the position of this point could be selected to characterize the change in the maximum intrusion depth of the drill teeth (Fig. 9c). In the modeling process, the longitudinal section of the drilling tooth formation along the midline was selected for analysis (Fig. 9d).

Fig. 10 shows the load on the bit under the action of conventional drilling and different types of impact drilling technologies. The details are as follows. a) During conventional drilling, the load transmitted to the bit through the drill string is the static load acting on the drill teeth. Under the action of the rotational device, the drill bit rotates at a constant speed, which causes the drill teeth to rotate at a certain rate, resulting in a displacement load, as shown in Fig. 10a, b) During rotary impact drilling, in addition to the above static and displacement loads, the stress wave generated by the axial impact drilling tool is transmitted to the bit from the axial direction, as shown in Fig. 10b, c) During torsional impact drilling. along with the above static and displacement loads, the torsional hammer produced tangential stress waves during the impact process, as shown in Fig. 10c, d) During axial-torsional coupled impact drilling, all the loads mentioned above act on the drill bit simultaneously. The mechanical environment of the drill teeth is also the most complex, as shown in Fig. 10d.

3.2. Numerical model

3.2.1. Geometric model and mesh generation

Based on the model above, the corresponding numerical model consisting of a PDC cutter and hard formation was developed, as shown in Fig. 11. As the deformation of the drill teeth was not considered in the calculation process, the drill teeth were set as a rigid body (Liu et al., 2020; Zhang et al., 2020, 2021). The size of the PDC cutter was set as φ 16 mm \times 4 mm, which is consistent with the size of the drill teeth in practical engineering applications. The size of the hard formation was set as 300 mm \times 16 mm; its length was sufficient for the migration time of the drill teeth.

The grid size would affect the calculation efficiency and the accuracy of the calculation results. In view of this, the trial

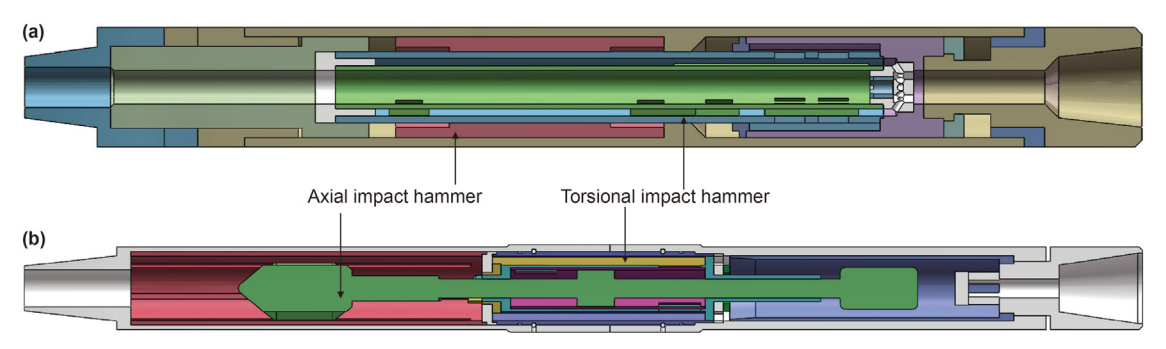


Fig. 3. Different types of axial-torsional coupled impact drilling tool structures.

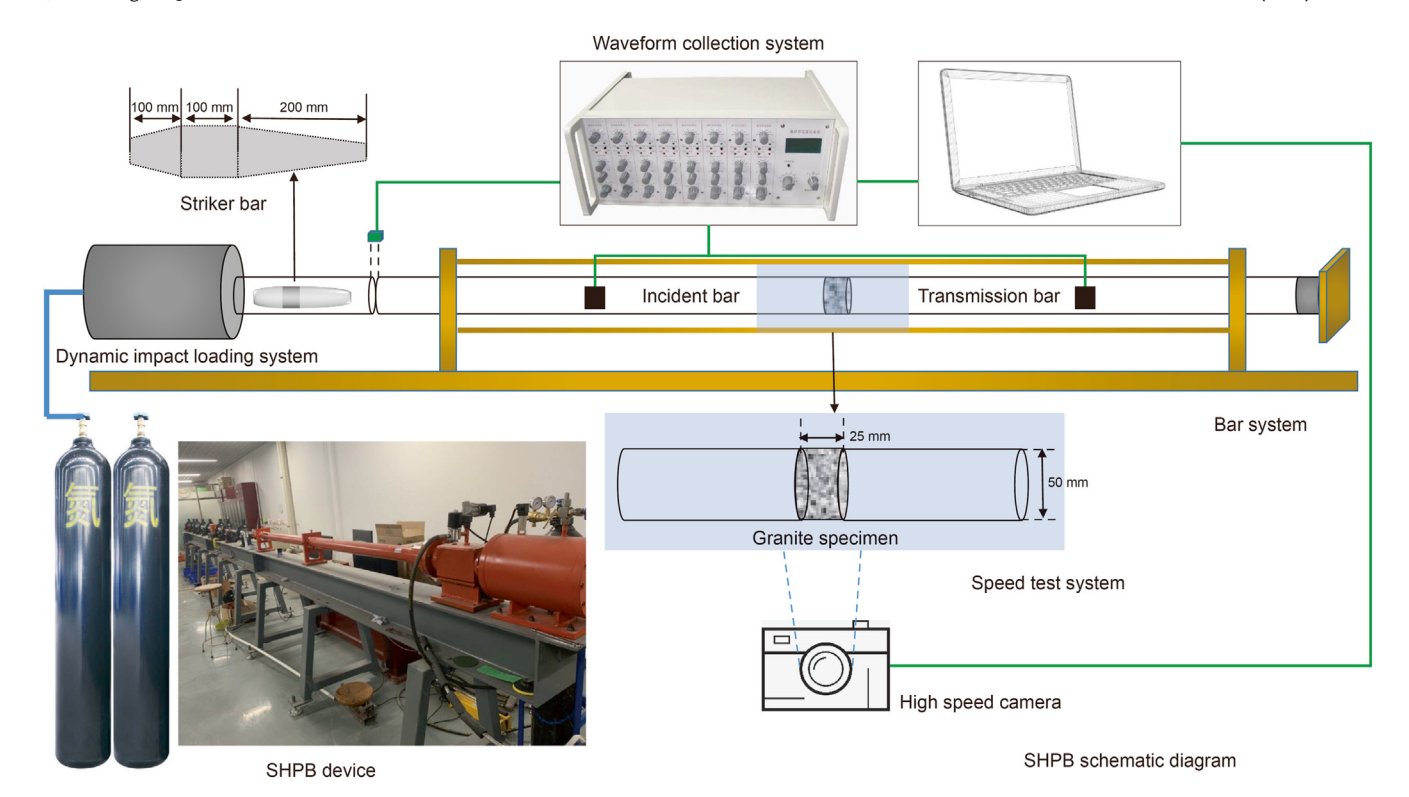


Fig. 4. SHPB experimental device.

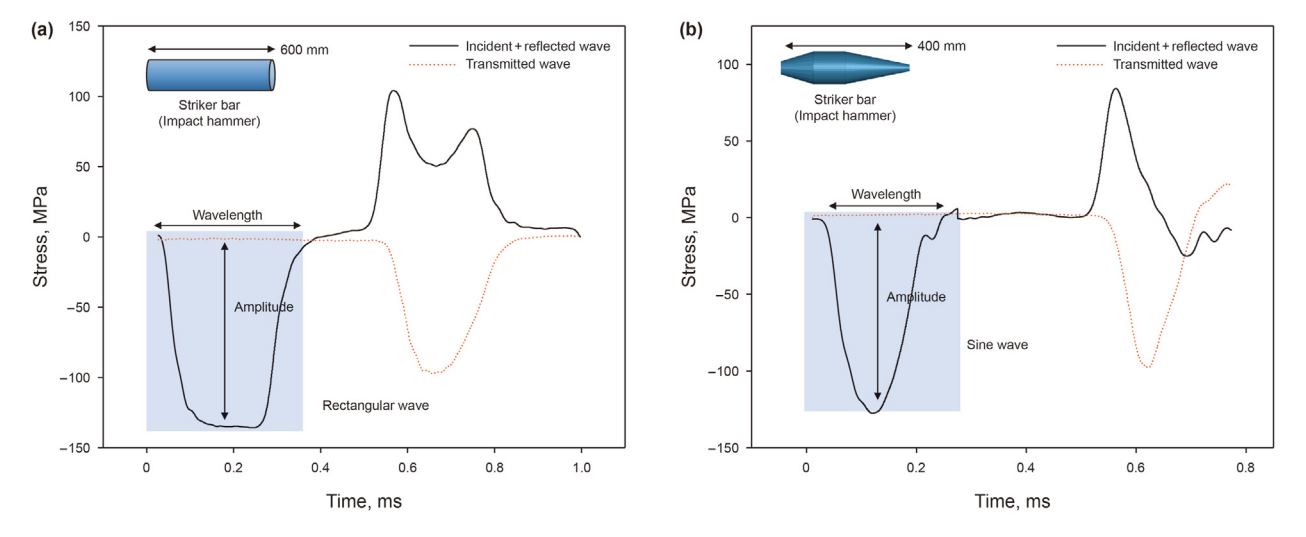


Fig. 5. Waveforms produced by striker bars of different shapes.

calculation of the established model showed that when the grid length and height were greater than 3 mm, the calculation results were discrete. Considering the calculation efficiency, the rock was divided into 600 elements horizontally, the length of the grid was 0.5 mm, and the variable density method was used to divide it into 20 elements longitudinally, the minimum and maximum height of the grid were 0.2 mm and 1 mm. Then the total number of rock model elements is 12000. The mesh division of cutting teeth is 20×60 , a total of 1200 elements.

3.2.2. Material specifications

Previous studies have shown that considering the dynamic rock characteristics during the process of impact rock-breaking can improve the analysis of the rock-breaking process (Baranowski et al., 2020; Xi et al., 2021). The RHT material model, which considers the impact of the strain rate, strain hardening, and damage softening, was proposed in previous studies. The verified dynamic parameters of granite, which is a typical hard rock, were used in the simulation of this study (Xi et al., 2021, 2022), as shown in Table 1. In verifying the numerical simulation results, the change rule of the stress-strain curve of the indoor test and numerical simulation results were used to compare and verify the accuracy of numerical models. The figure shows that the two curves have good consistency (Fig. 12a, b).

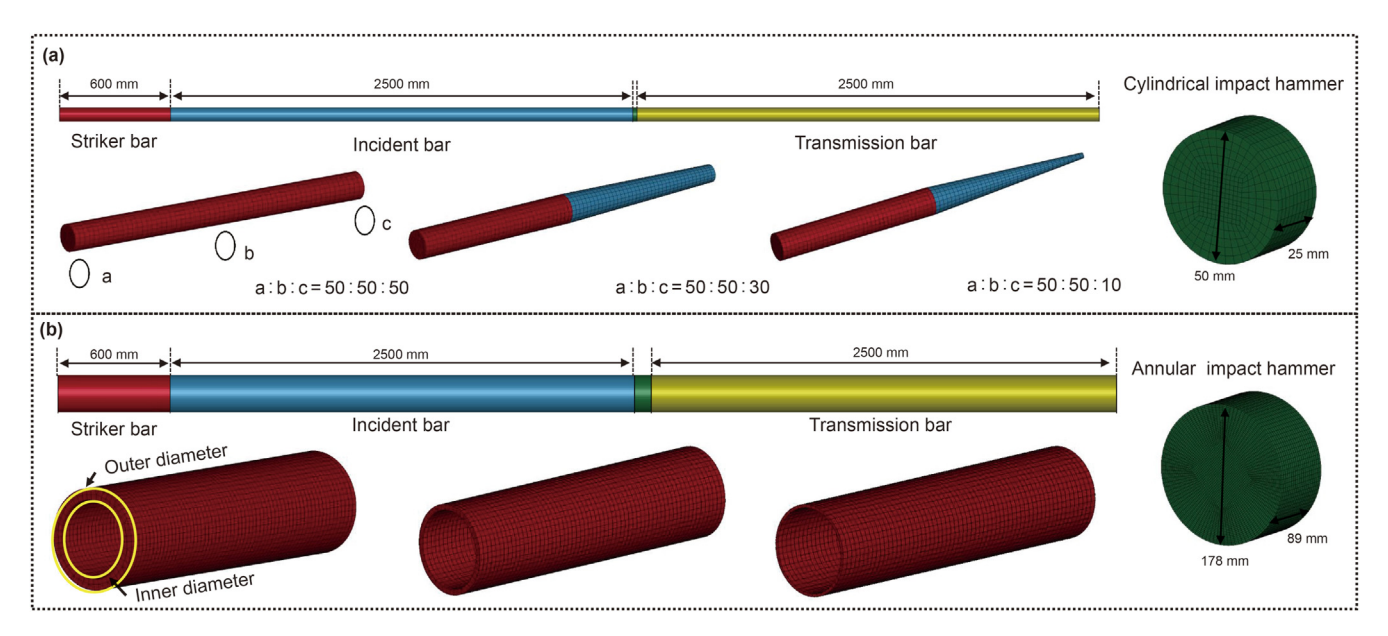


Fig. 6. Numerical model of the SHPB test.

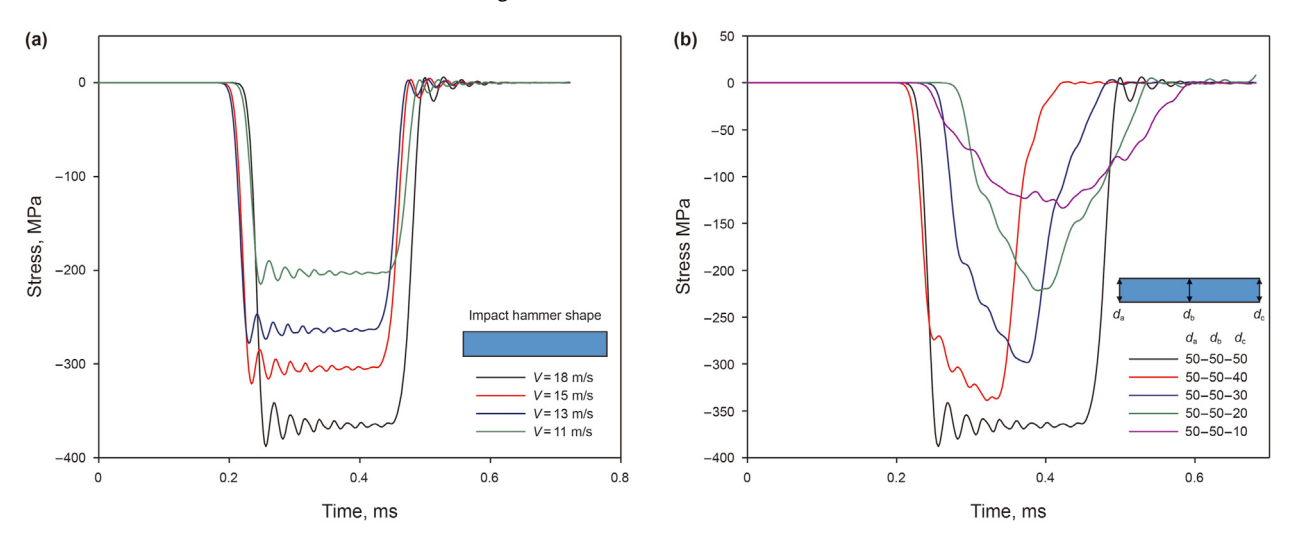


Fig. 7. Incident wave of cylindrical impact hammer. (a) Incident wave under different impact velocities; (b) Incident wave under the action of the hammer with different shapes.

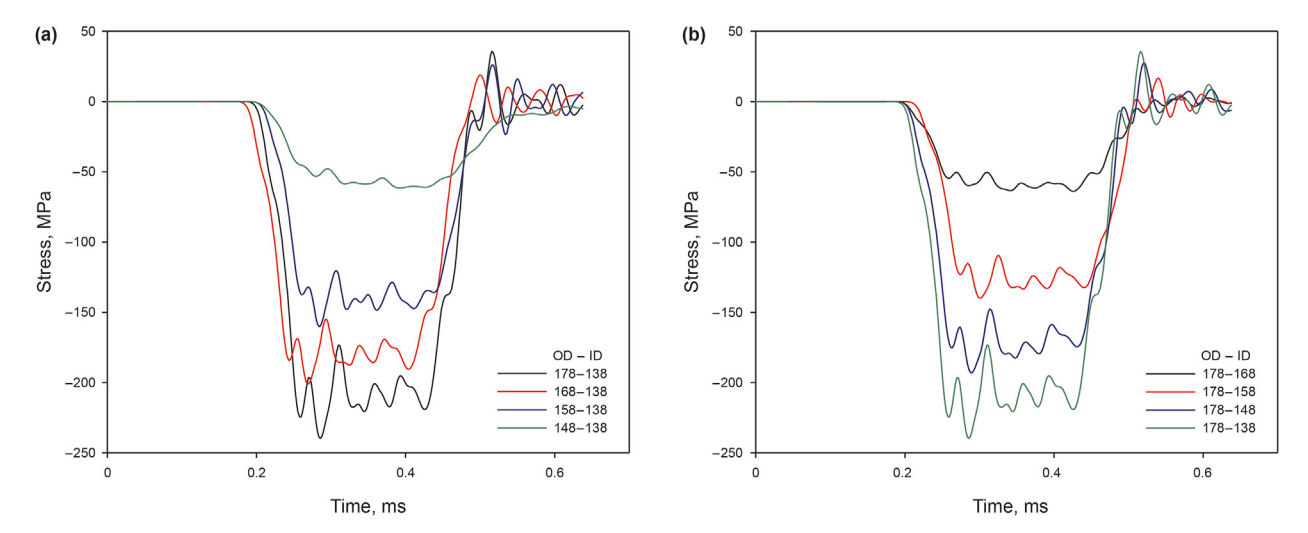


Fig. 8. Incident wave of annulus impact hammer. (a) Change the outer diameter without changing the inner diameter; (b) Change the inner diameter without changing the outer diameter.

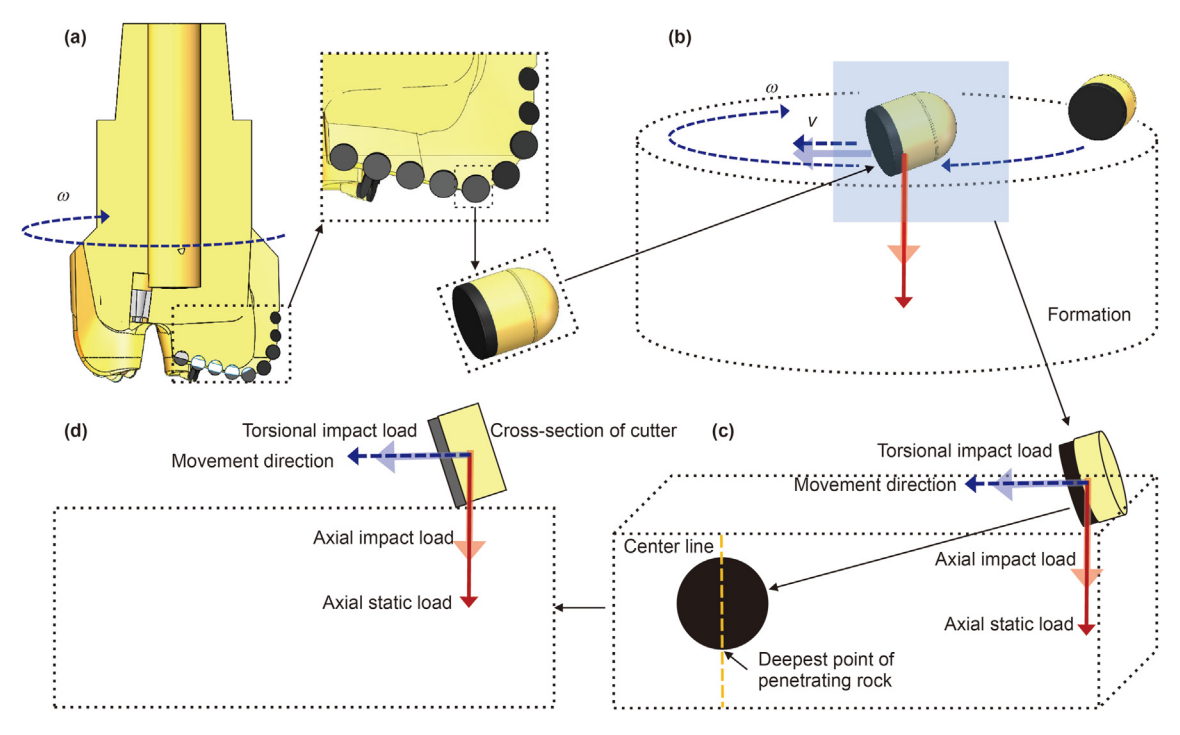


Fig. 9. Engineering model.

3.2.3. Load application and boundary condition

Based on actual drilling conditions, the boundary conditions of the numerical model were set as shown in Fig. 13. a) The inclination angle between the PDC cutter and formation was set as 20° , which remained constant during the movement of the cutter. b) The two sides and bottom of the rock were set as non-reflection boundaries

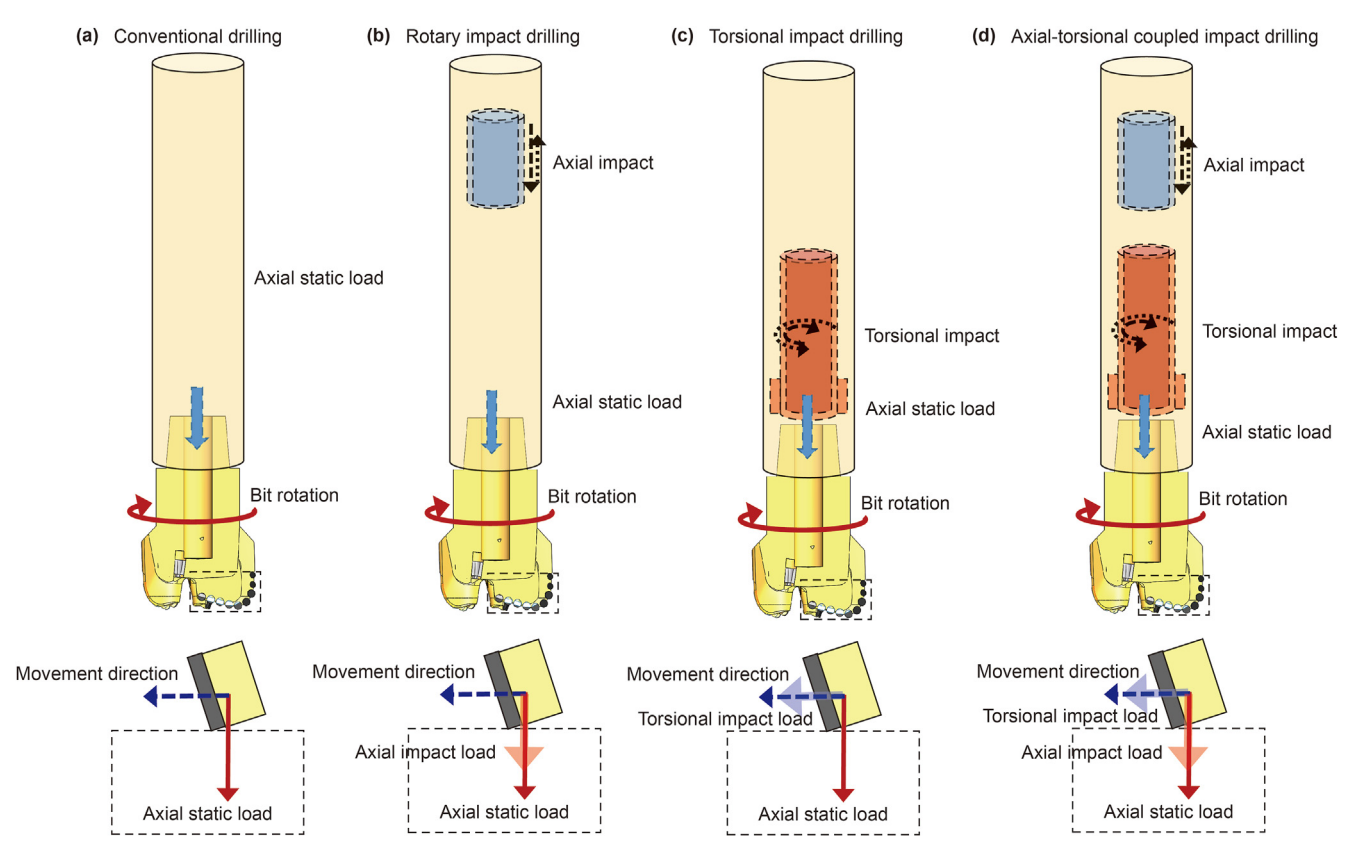


Fig. 10. Engineering model of conventional and different types of impact drilling methods.

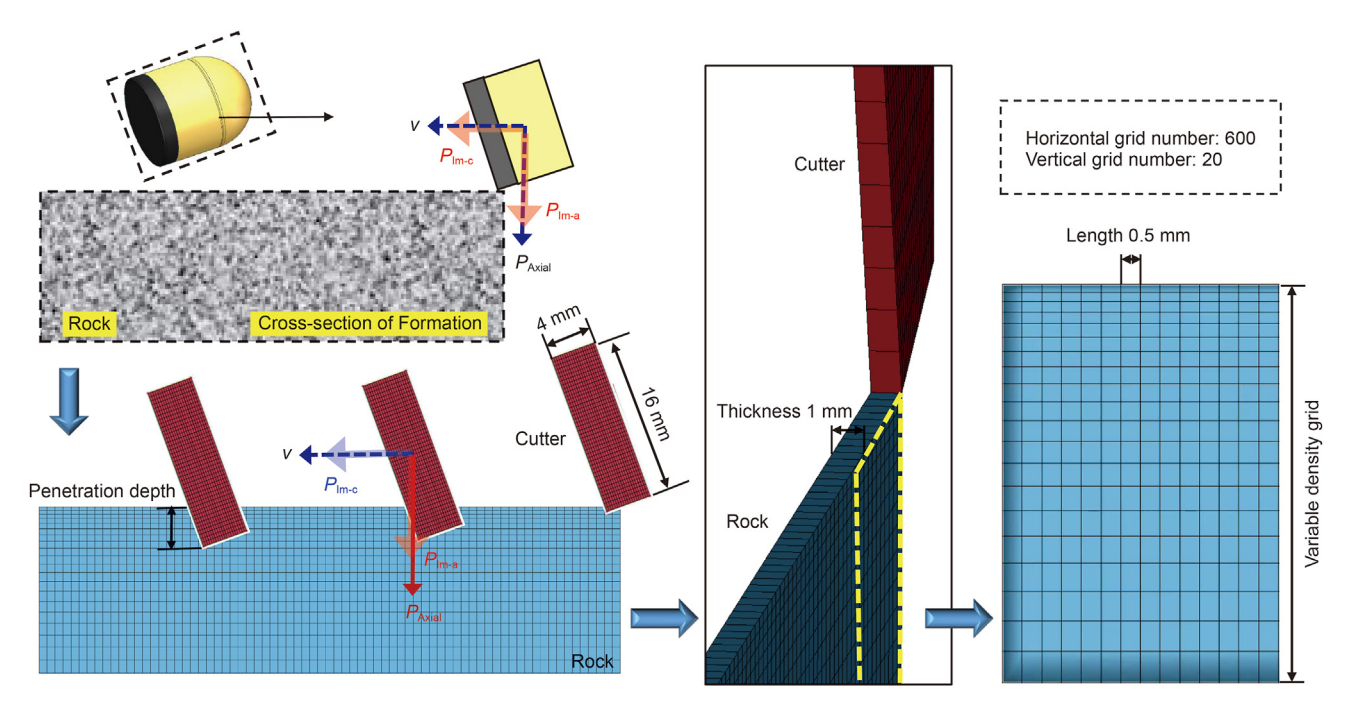


Fig. 11. Numerical model.

to characterize the stratum as an infinite boundary, which was consistent with the actual project. c) The hard stratum in its original state remained intact. The PDC drill teeth made contact with the formation before drilling but did not invade; hence, the penetration depth of the drill teeth during the rock-breaking process could be calculated from scratch and used to describe the mechanical penetration rate to a certain extent.

The load parameters of the model were set as follows. First, the axial static load transmitted from the drill string to the bit remained constant. Second, the axial and torsional impact hammers generated axial and torsional stress waves on the bit. The waveform of the generated stress wave was set as a rectangular wave. To analyze the influence of the axial and torsional shock loads on the rockbreaking effect, the amplitude, frequency, wavelength, and phase

difference of the two types of waves were varied, as shown in Fig. 14a.

According to the above analysis, the axial load borne by the drill teeth is the sum of the static and dynamic loads caused by the axial impact (F_{WOB} , f_{Im-a}). The tangential load is the impact load caused by the torsional impact (f_{Im-c}), as shown in Fig. 14b. The drill string drove the rotation of the drill bit. The PDC drill teeth maintained a certain speed to generate a displacement load that could be calculated according to the speed of the drill bit and the relative position of the drill teeth.

On the basis of drilling engineering, a drill bit with a diameter of φ 215.9 mm was selected, and the research object was the PDC cutter positioned at the edge of the bit. In the drilling process, the rotational speed of the bit was set as 60 RPM, while the tangential

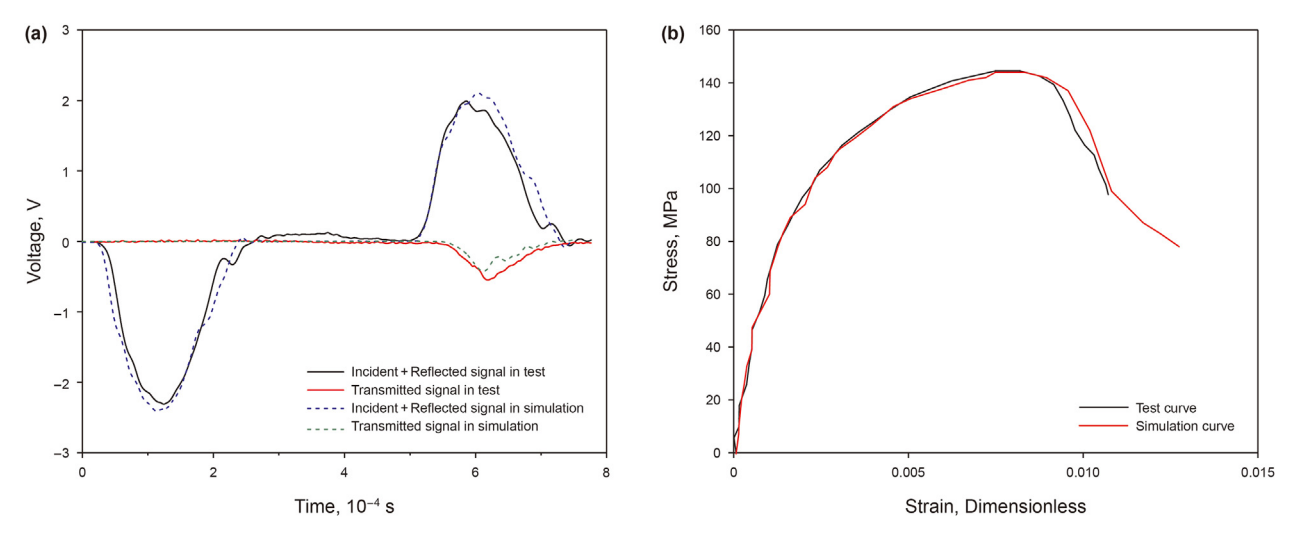


Fig. 12. Comparison of simulation and test results. (a) Input load; (b) Stress-strain curves.

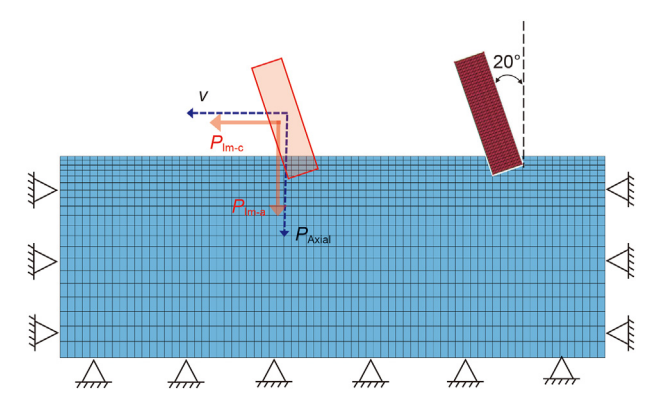


Fig. 13. Boundary condition.

velocity of the research object was approximately 0.68 m/s.

4. Verification of numerical simulation

4.1. Comparison of cutting surfaces

According to the developed numerical model, the change in the displacement of the drill teeth in the Y-direction was extracted and

used to characterize the penetration depth of the PDC cutter, as shown in Fig. 15. As seen in the figure, even in conventional drilling, the cutting surface is extremely rough, and the penetration depth fluctuates. The rock area passed by the PDC cutter has an irregular sawtooth shape, suggesting that the contact area between the drill teeth and cutting plane constantly changes. The main reason for this is that despite the static load applied in the Y-direction, the contact area changes with the movement of the drill teeth during the interaction between the cutting teeth and rock, contributing to the continuous change in the penetration depth.

Cheng et al. (2019) conducted linear cutting tests using a PDC cutter with a back rake angle of 20° and reconstructed the cutting groove, as shown in Fig. 16. AA' is the section parallel to the central axis at the bottom, which can be used to represent the change in penetration depth. It can be observed that even under the action of linear cutting, the penetration depth at the rock bottom continued to fluctuate significantly, which qualitatively supports the simulation results.

4.2. Rock-breaking mechanism of conventional drilling

A previous study (Cheng et al., 2019) demonstrated the rockcutting process by the PDC cutter, which can be summarized as follows. a) The PDC cutter intrudes into the rock at a certain depth and makes contact with the rock before the cutter. Because the

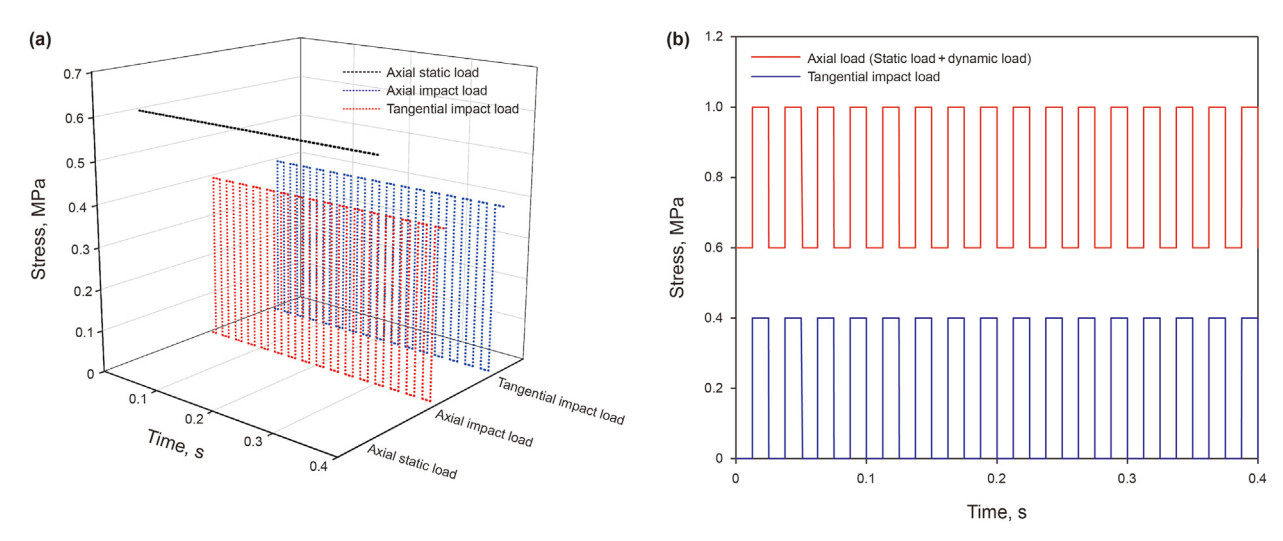


Fig. 14. Load curves of different waveforms.

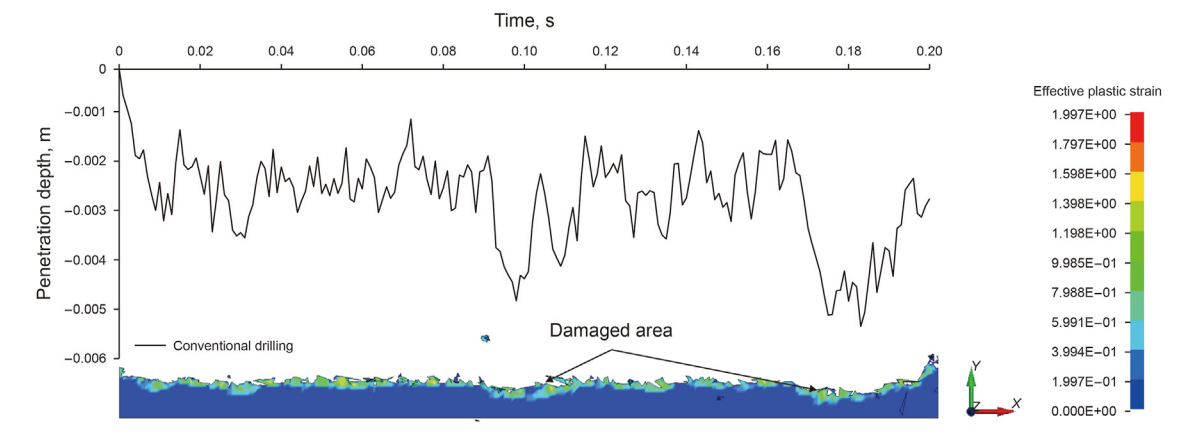


Fig. 15. Penetration depth in conventional drilling.

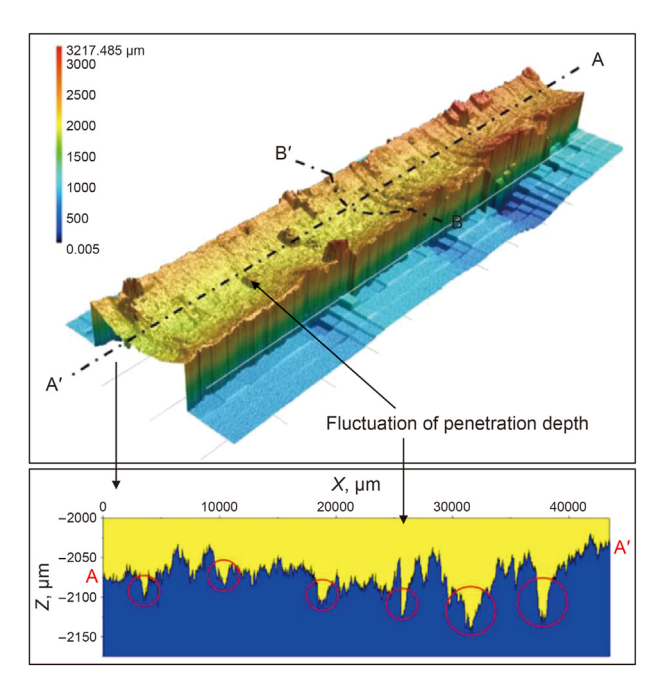


Fig. 16. The reconstructed cutting groove (Modified from Cheng et al. (2019)).

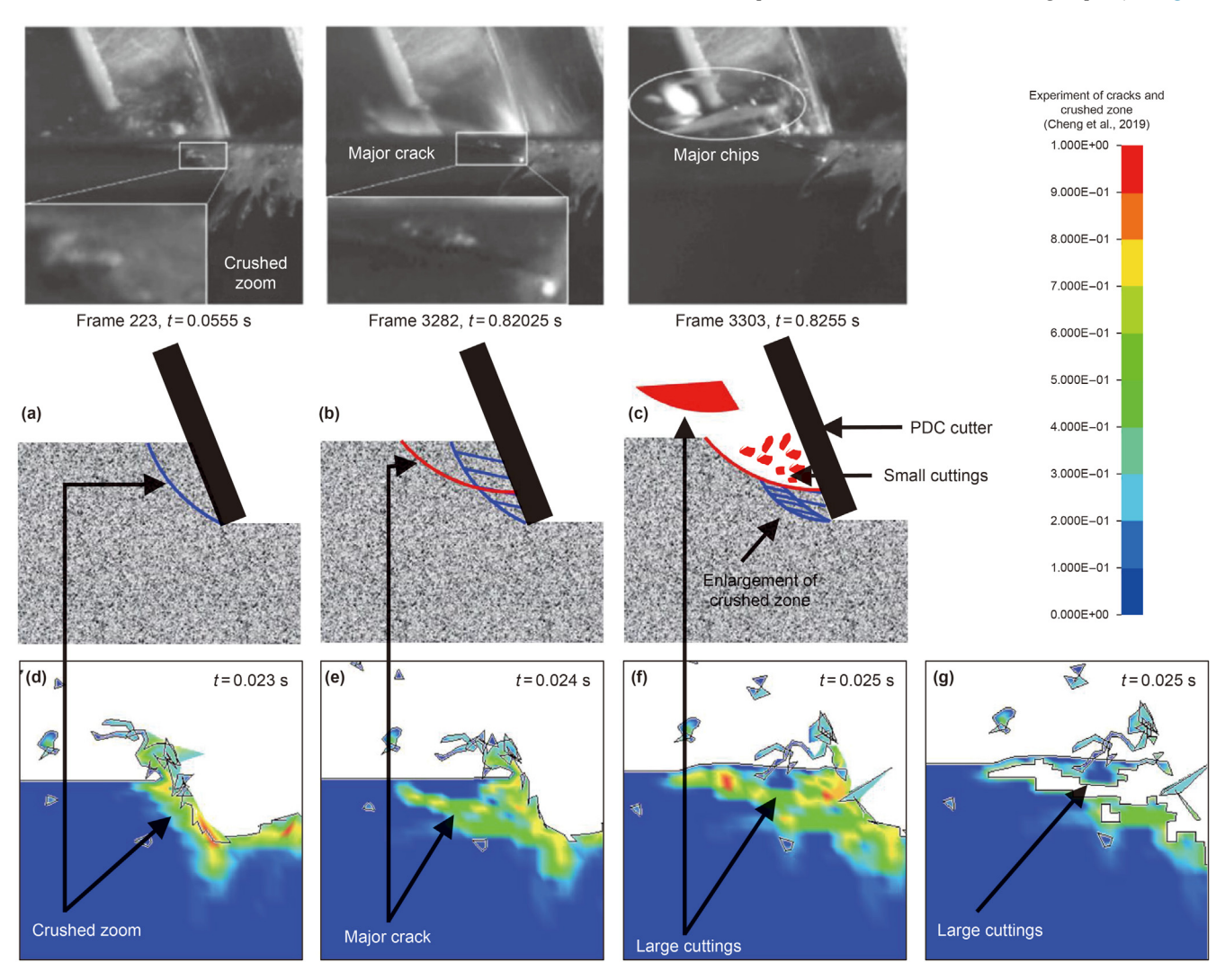
torque of the drill bit acts on the rock, a crushed zone slowly formed due to the compression of the cutter, as shown in Fig. 17a, b) After a comparatively long crushing process, a large crack formed due to tension or shear, as shown in Fig. 17b, c) When a major chip separates from the rock matrix, the force that prevented the PDC cutter from moving forward was reduced, causing the PDC cutter to move abruptly, which significantly enlarged the crushed zone, as shown in Fig. 17c.

Fig. 17d—f show the numerical simulation results in different periods (0.023—0.025 s), which can reflect the transient process of rock cutting by drill teeth. The numerical simulation results agreed with the rock-breaking mechanism, further proving the accuracy of employing the rock dynamics method to investigate the rock-breaking process.

Fig. 17f and g show the rock-cutting process with the PDC cutter. The difference is that elements with a degree of damage of over 75% were eliminated to represent the cracks below the cutting surface. It can be observed that large rock cuttings were stripped from the hard rock body, which is consistent with the large rock cuttings in the experimental results.

4.3. Cracks below the cutting surface and cuttings

Based on the results of previous experiments, the damage extended deeper into the rock than the cutting depth (Cheng et al.,



 $\textbf{Fig. 17.} \ \ \textbf{Rock-breaking process with a PDC cutter.}$

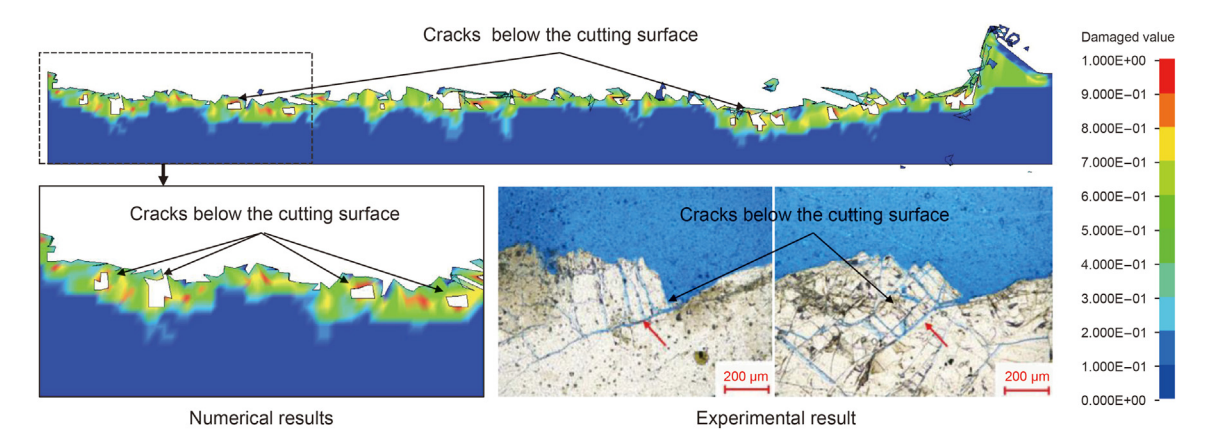


Fig. 18. Cracks below the cutting surface.

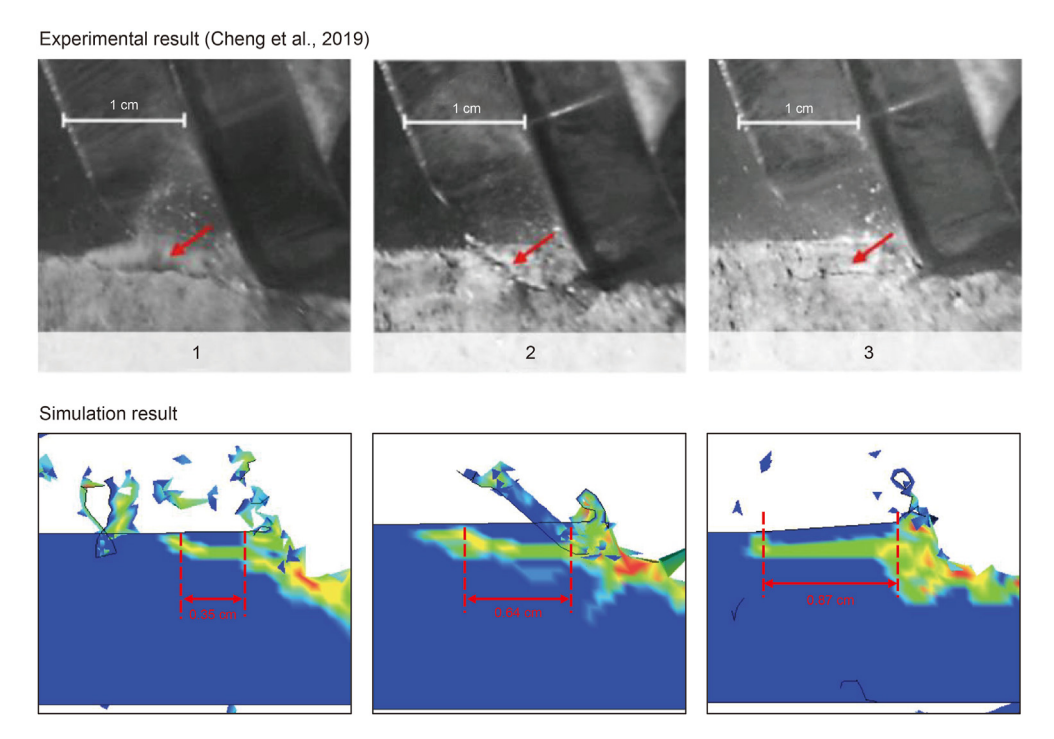


Fig. 19. Comparison of rock failure modes.

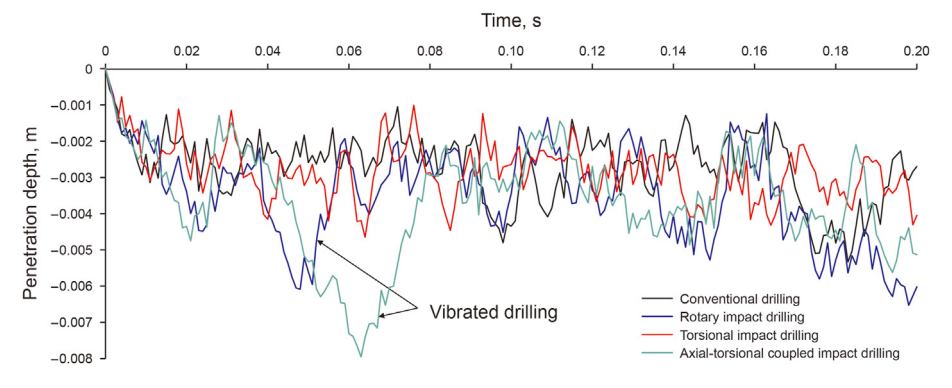


Fig. 20. Comparison of penetration depths under different drilling methods.

2019), as shown in Fig. 18. To further analyze the cracks under the cutting surface, elements with a degree of damage degree of over

75% were eliminated; hence, the cracks below the cutting surface were the missing elements. Fig. 18 shows the numerical simulation

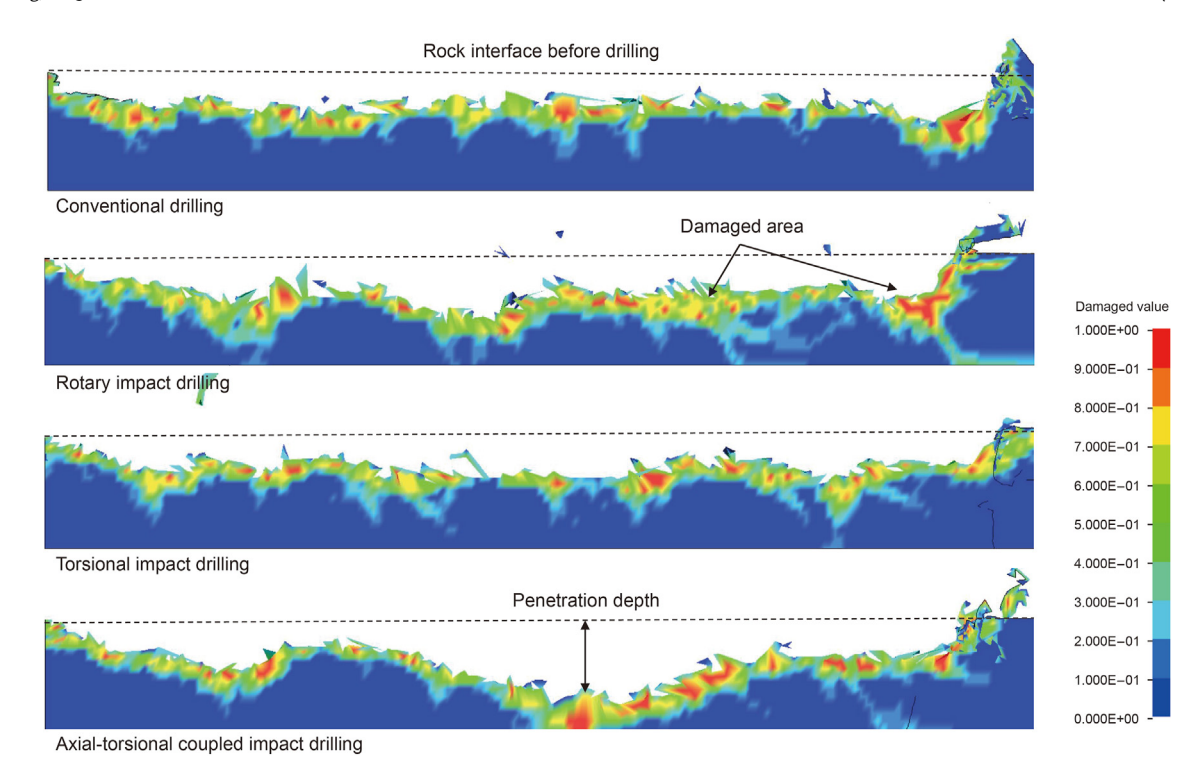


Fig. 21. Comparison of the damaged area under different drilling methods.

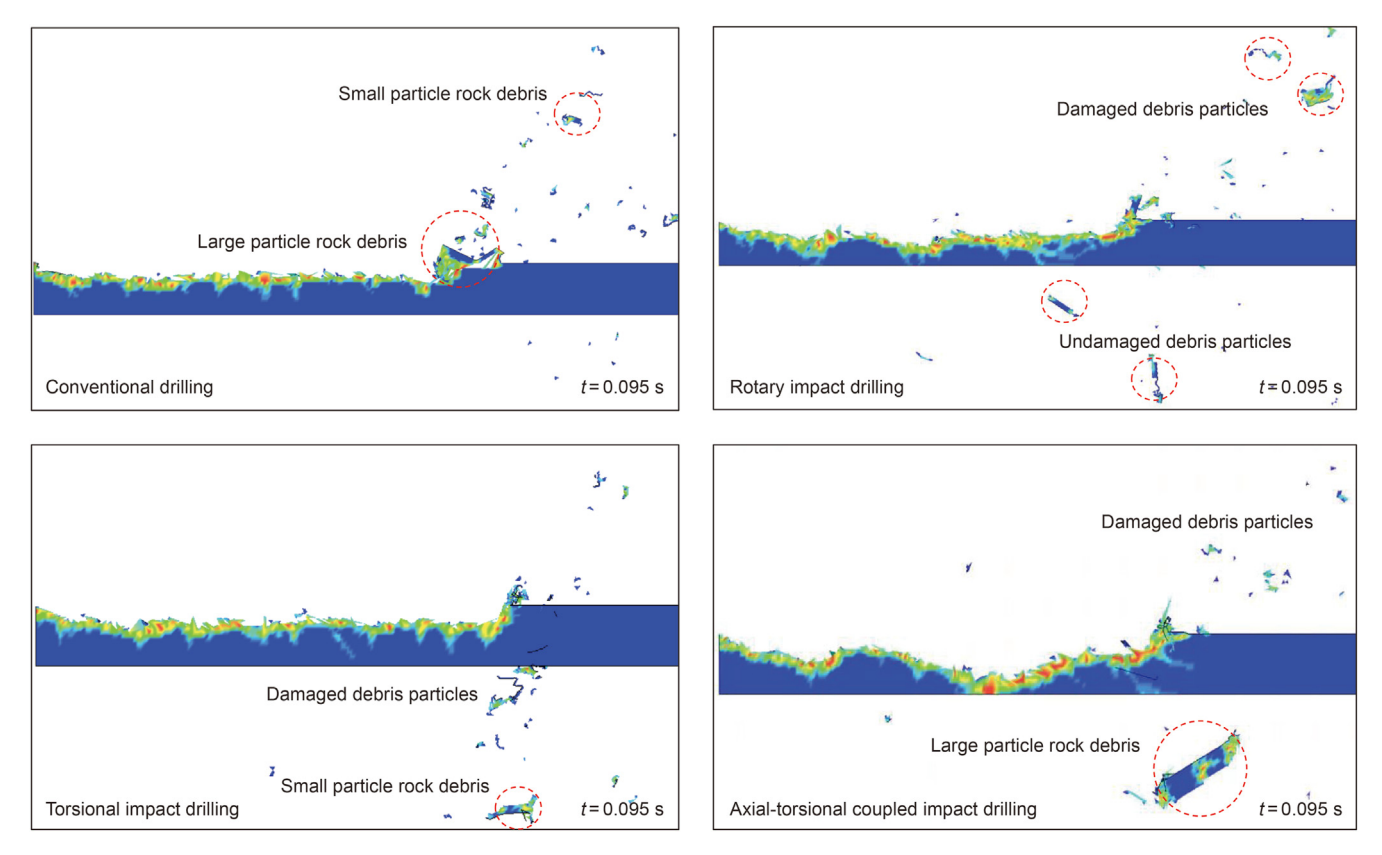


Fig. 22. Comparison of debris under different drilling methods.

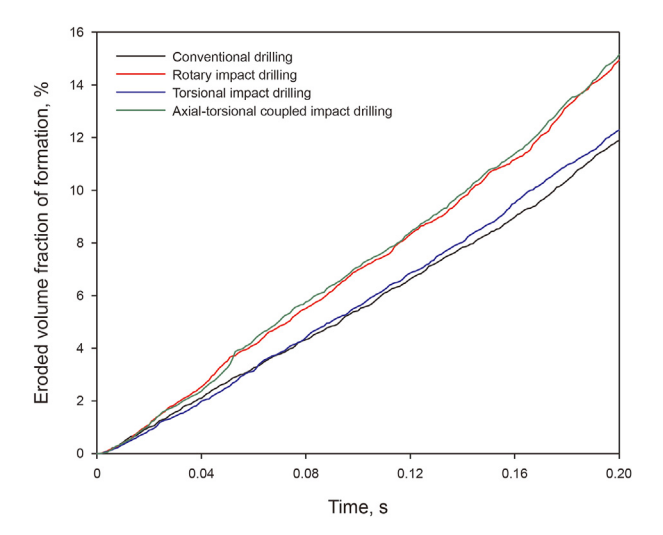


Fig. 23. Comparison of eroded volume under different drilling methods.

results, in which apparent cracks occurred below the cutting surface, which is consistent with the experimental results.

Based on the experiments of Cheng et al. (2019), a high-speed camera was used to record the significant cracks in the rock. A comparison of this data with the numerical simulation results in this study (Fig. 19) showed that after the PDC drill teeth intruded

into the hard rock mass, the rock mass was sheared under the action of the displacement load. Under shear action, microcracks appeared on the rock mass and began to peel off. Comparison of the laboratory test and numerical simulation results showed good agreement, and accurately reflected the rock-breaking process. It should be noted that in the two types of results, the shape of the cracks and the morphology of rock debris fragments that peeled off were all similar, further proving the accuracy of the numerical simulation results.

5. Comparison of penetration depth and sensitivity analysis

5.1. Comparison simulation results in different drilling methods

5.1.1. Comparison of penetration depth

The penetration depth of the PDC cutter using different drilling methods (i.e., conventional, rotary impact, torsional impact, and axial-torsional coupled impact drilling) were obtained and compared, as shown in Fig. 20. Based on the variations in the penetration depth and amplitude fluctuations, the following observations were made.

 a) During conventional and torsional impact drilling, the drill teeth were only subjected to an axial static load in the axial direction. Although the penetration depth of the drill teeth fluctuated to some extent, the amplitude fluctuations were slight, indicating that the drill bit was relatively stable during drilling.

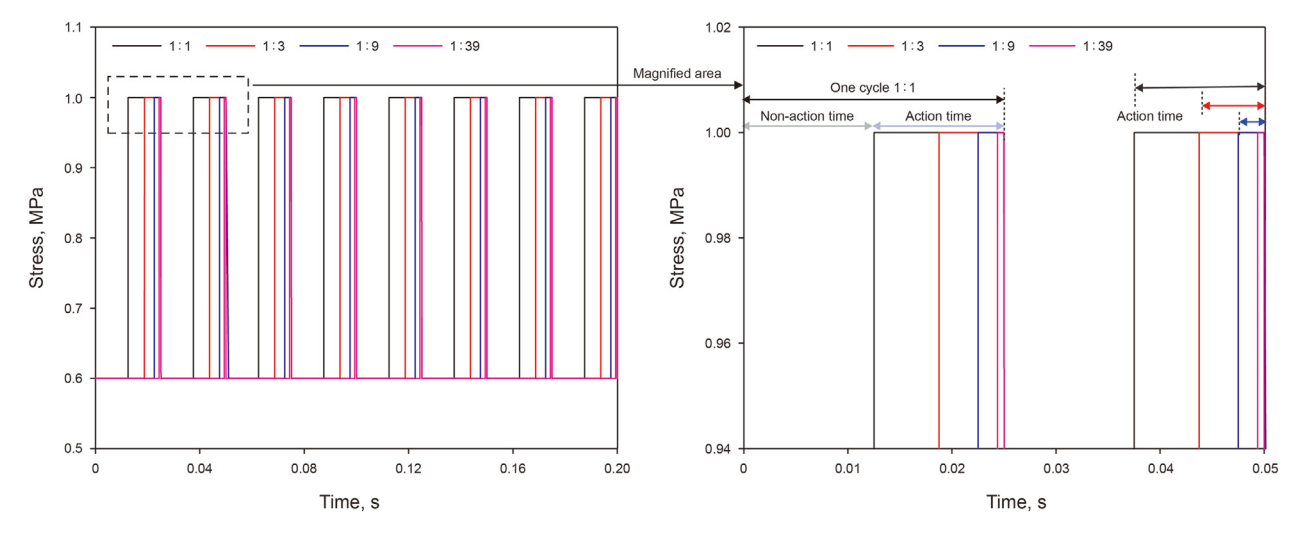


Fig. 24. Action time and non-action time parameter settings.

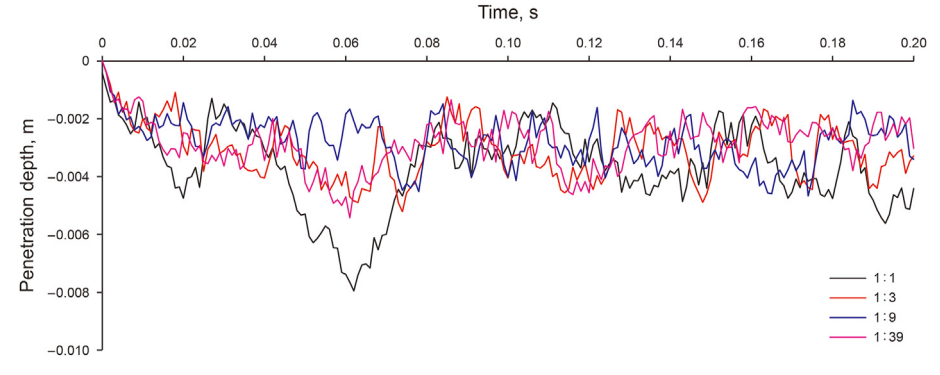


Fig. 25. Penetration depth under the different action time and non-action time ratios.

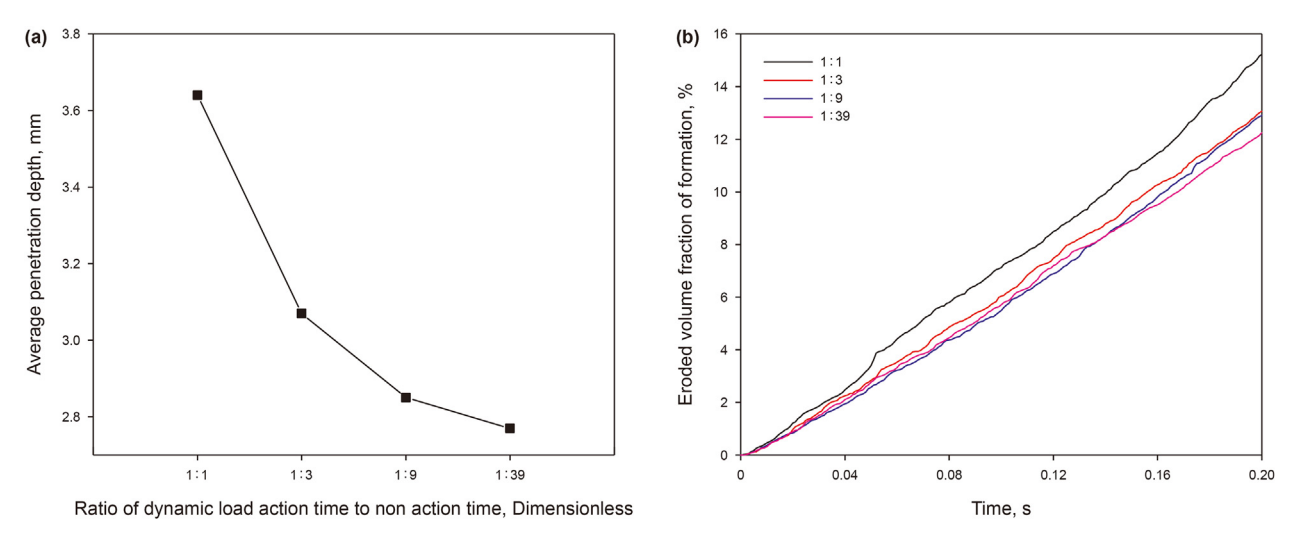


Fig. 26. Simulation results under the different ratios of action time and non-action time.

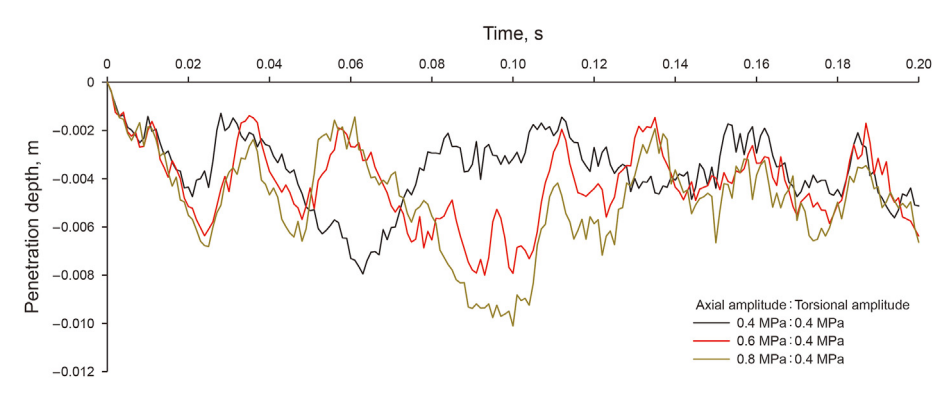


Fig. 27. Penetration depth under different axial impact amplitudes.

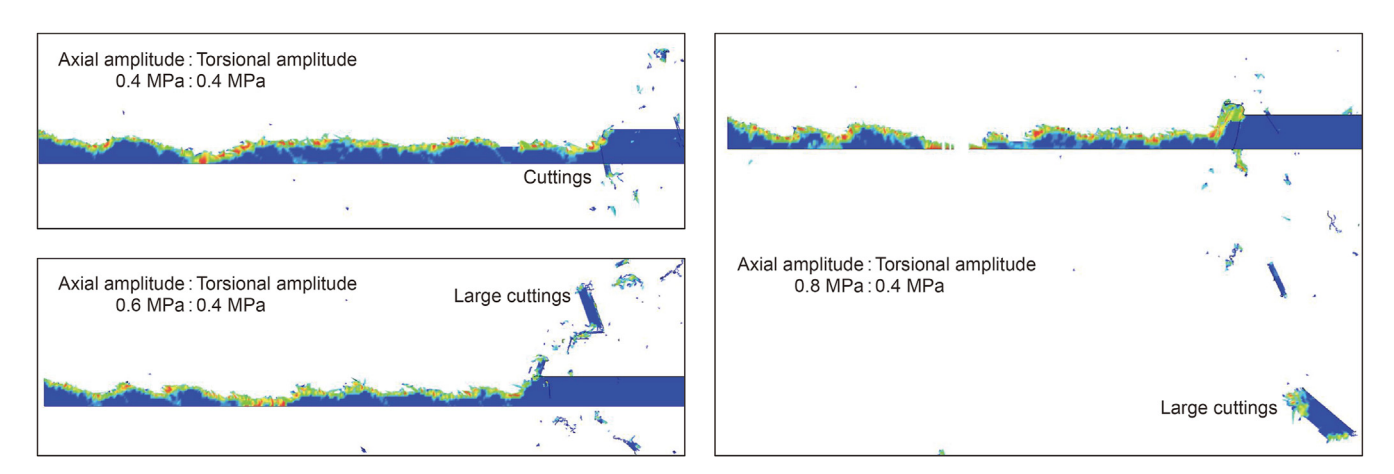


Fig. 28. Debris under different axial impact amplitudes.

b) As seen during rotary impact and axial-torsional impact drilling, the fluctuations of the penetration depth were exacerbated by the application of an axial impact load to the drill bit. This is because the axial dynamic load was applied to the drill bit when the PDC cutter moved to a specific position. Subsequently, the penetration depth significantly increased under the combined axial static and dynamic loads. The average penetration depths of conventional drilling, rotary, torsional, and axial-torsional coupled impact drilling is 2.68 mm, 3.52 mm, 2.83 mm, and 3.61 mm, respectively. It can be seen that among these different drilling methods, the axial-torsional coupled impact drilling method has the best effect in terms of penetration depth, followed by rotary impact, torsional impact, and conventional drilling. Compared with conventional drilling, the average

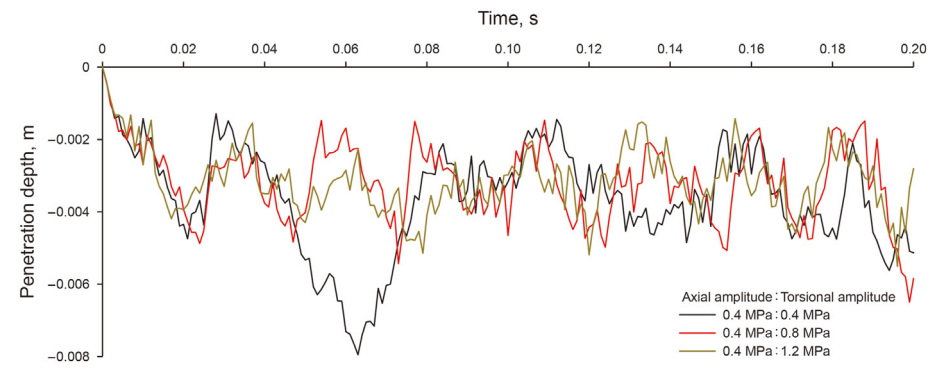


Fig. 29. Penetration depths under different torsional impact amplitudes.

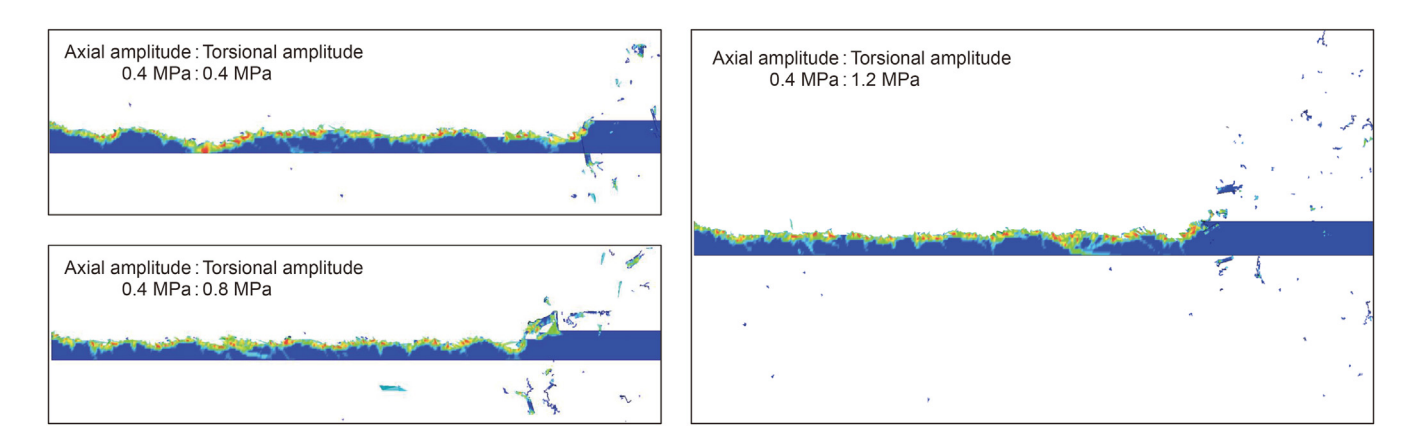


Fig. 30. Debris under different torsional impact amplitudes.

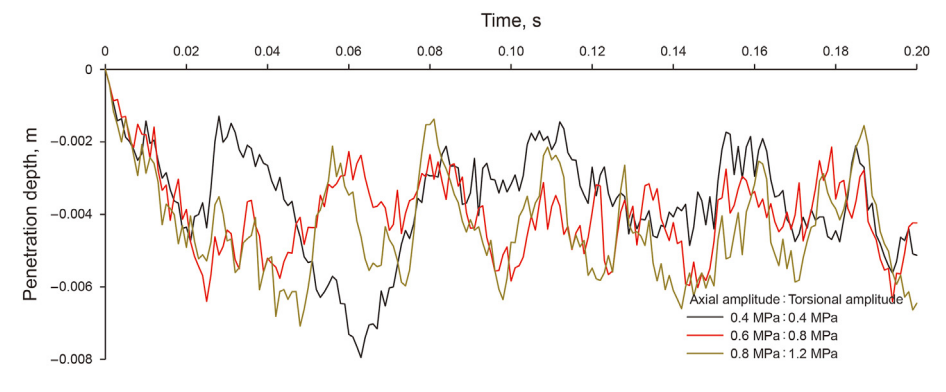


Fig. 31. Penetration depths under different torsional impact amplitudes.

penetration depth of the torsional coupled and rotary impact drilling increases by 34.7% and 31.3%, respectively. It indicates that the axial impact load is the main decisive factor affecting the penetration depth, and the ROP raising effect of the axial-torsional coupled impact drilling technology is the most obvious.

5.1.2. Comparison of damaged area and debris

(1) Comparison of damaged areas

In the rock-breaking process, the PDC cutter cuts the rock and damages the rock below the cutting surface, which directly affects the subsequent rock-breaking effects and influences the service life of the bit. The rock-breaking process within the first 0.1 s was

selected for analysis, as shown in Fig. 21. It can be observed that the rock below the cutting surface was damaged by different impact drilling methods. Among these, the damaged area below the cutting surface caused by rotary impact drilling was the most evident, followed by torsional impact drilling and conventional drilling.

It can be seen that the additional impact load damaged the rock below the cutting surface and reduced the strength of the rock. When the drill teeth rotated back to this position, it was easier for the drill teeth to break the rock. The reaction force borne by the drill teeth decreased, which will improve the service life of the drill bit.

(2) Comparison of cutting size

The debris size produced during rock-breaking affects the

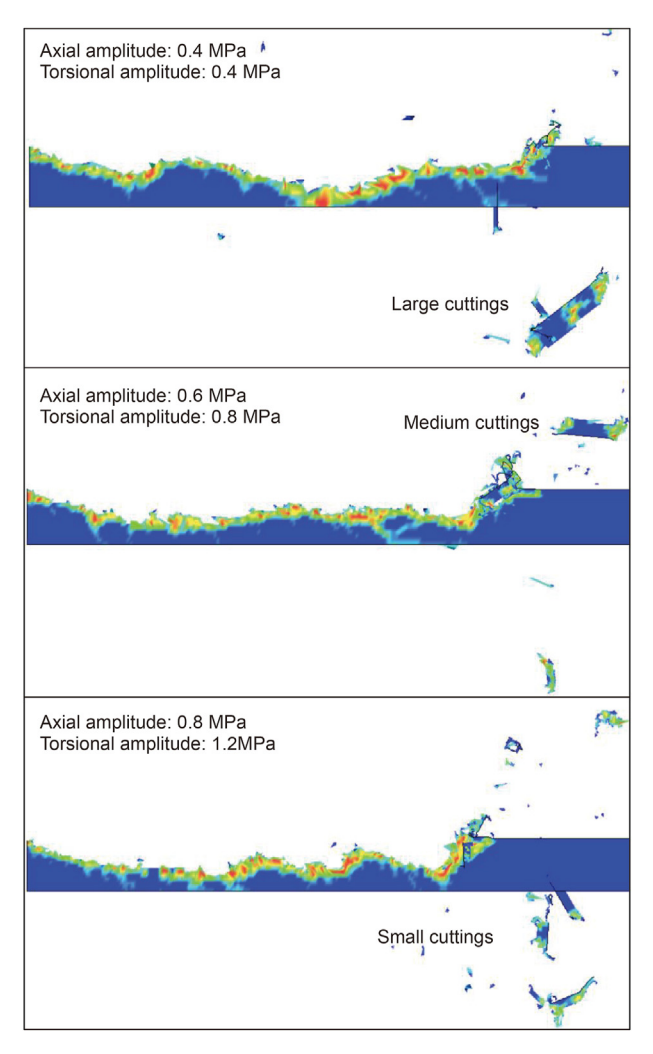


Fig. 32. Debris under axial and torsional impact amplitudes.

cleanliness of the wellbore; hence, the rock cuttings under different drilling methods were analyzed, as shown in Fig. 22. The simulation results showed that axial-torsional coupled impact drilling produced the most significant cuttings (1.22 cm), followed by rotary impact, conventional, and torsional impact drilling. An axial impact is more likely to produce large-particle rock cuttings, affecting the cleanliness of the wellbore. This indicates that it is essential to adjust the axial-torsional coupled impact drilling parameters to reduce the size of the rock cuttings.

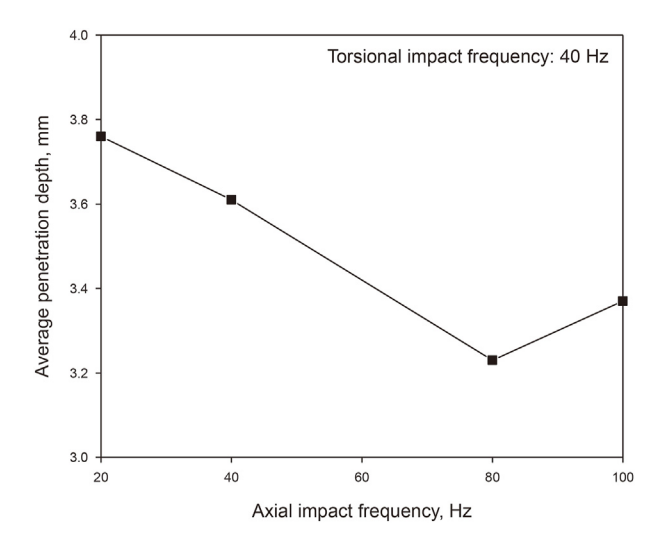


Fig. 34. Average penetration depth under different axial impact frequencies.

5.1.3. Comparison of the eroded volume of rock

Fig. 23 shows a comparison of the eroded volume fractions of the formation under different drilling methods. Compared with conventional drilling, the impact drilling methods increased the eroded volume of rock. The most significant was under axial-torsional coupled impact drilling, which increased the eroded volume by 27.4%, followed by rotary (25.6%) and torsional impact drilling (3.4%). This further proves that impact drilling methods, especially axial-torsional coupled impact drilling, can improve drilling efficiency.

5.2. Sensitivity analysis

5.2.1. Influence of wavelength

The wavelength is affected by the length of the impact hammer. Because the wavelength can be characterized as the action time under time threshold conditions, the period in which the hammer moves but does not hit the base is defined as the non-action time, while the sum of the action and non-action times is a cycle. To further analyze the influence of the wavelength on the rockbreaking effect, the impact cycle remained unchanged during the analysis. Only the ratio of the action time to the non-action time changed, as shown in Fig. 24.

Fig. 25 shows the penetration depth of the PDC cutter under different action and non-action time ratios. The penetration depth fluctuated significantly when the action time to non-action time ratio was large. As the ratio decreased, the amplitude fluctuation

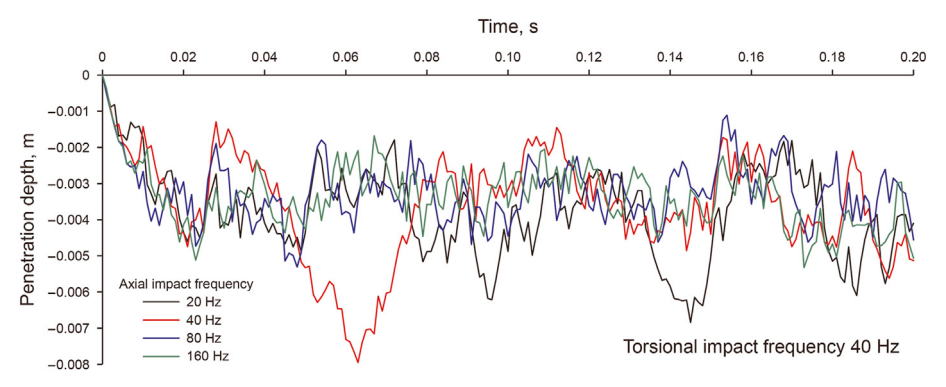


Fig. 33. Penetration depth under different axial impact frequencies.

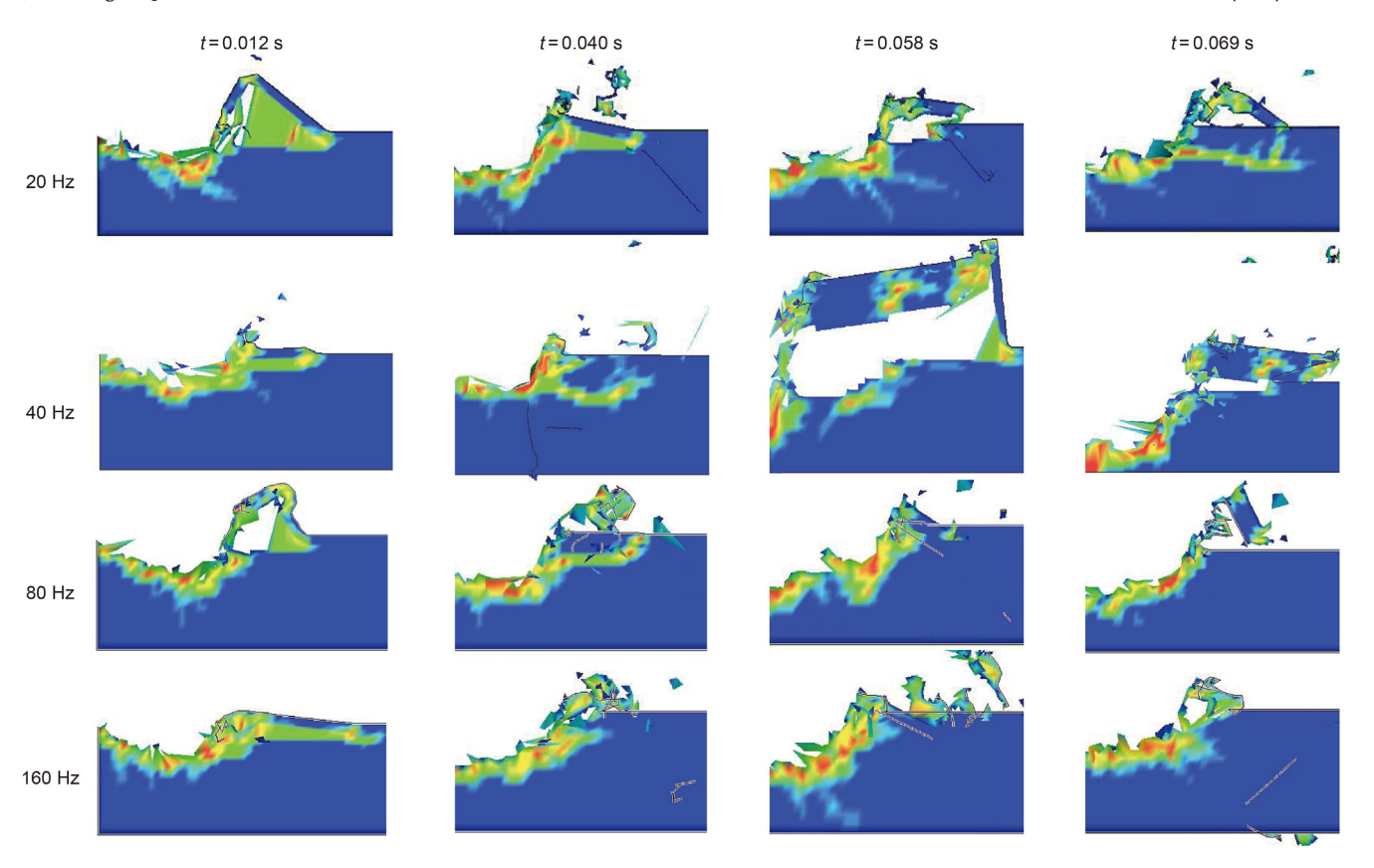


Fig. 35. Debris under different axial impact frequencies.

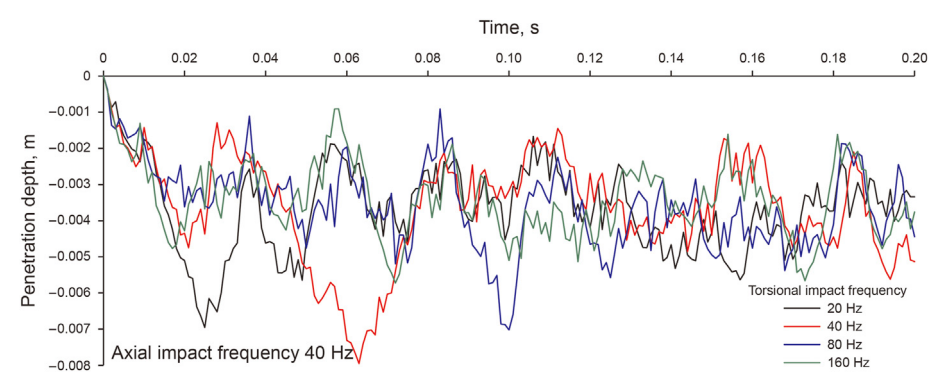


Fig. 36. Penetration depths under different torsional impact frequencies.

decreased. At action time to non-action time ratios of 1:1, 1:3, 1:9, and 1:39, the average penetration depths were 3.64 mm, 3.07 mm, 2.85 mm, and 2.77 mm, respectively. The average penetration depth decreased with the action time (wavelength), as shown in Fig. 26a. The rock-breaking volume, which can be obtained based on cutting depth and distance, exhibited a similar trend of decreasing with the action time (wavelength), as shown in Fig. 26b. Therefore, using an impact drilling tool with a long hammer in the vertical well section should be considered to increase the rock-breaking effect.

5.2.2. Influence of impact amplitude

The axial and torsional impact amplitudes affected the movement of the coupled impact drilling tool. To further analyze the influence of an amplitude change on the rock-breaking effect, the axial or torsional impact amplitudes should be changed separately to explore the impact of axial or torsional impact waves. Thus, the axial and torsional impact amplitudes were adjusted simultaneously, and their influence on the rock-breaking effect was analyzed.

(1) The torsional amplitude remained unchanged, and the axial impact amplitude changed.

The initial amplitude of the axial and torsional impact loads was 0.4 MPa. Fig. 27 showed the rock-breaking effects when the amplitude of the torsional impact load remained unchanged, while that of the axial impact load changed. It can be observed that as the amplitude of the axial load increased, the vibration amplitude of the penetration depth became significant. In this case, the average

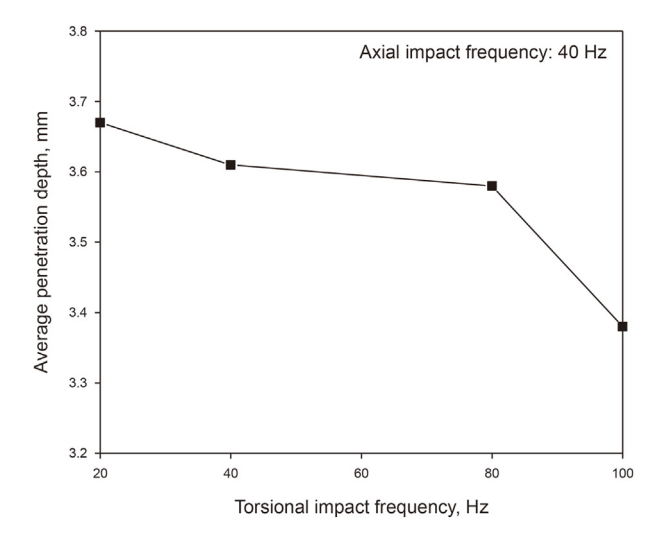


Fig. 37. Average penetration depth under different torsional impact frequencies.

penetration depths were 3.61 mm, 4.24 mm, and 4.90 mm. The axial load significantly influences the depth of the cutting teeth. However, as the axial load increased, the diameter of the rock cuttings formed by crushing increased (Fig. 28), and the maximum

size reached 1.6 cm \times 0.68 cm, affecting the cleanliness of the wellbore.

(2) The axial amplitude remained unchanged, and the torsional impact amplitude changed.

In conventional drilling, when the penetration depth of drilling teeth is deep, the volume of cuttings is more significant, and the cutting force required for rock breaking increases. When the cutting force is not enough to break the rock, the phenomenon of cyclic accumulation and release of cutting force appears, which is called stick-slip vibration. The previous research results show that applying load in the torsional direction can effectively solve this problem (Xi et al., 2022).

The rock-breaking effects were analyzed when the axial load remained unchanged (0.4 MPa) and the torsional impact loads (0.4 MPa, 0.8 MPa, and 1.2 MPa) were changed. As the torsional impact load increased, the penetration depth fluctuations decreased, as shown in Fig. 29. When the torsional impact loads are 0.4 MPa, 0.8 MPa, and 1.2 MPa, the average penetration depths are 3.61 mm, 3.18 mm, and 3.15 mm, respectively. The average penetration depth decreased as the torsional impact load increased. This was attributed to the increasing tangential load, which changed the combined vector value of the bidirectional load and reduced its role in the axial direction. At the same time, it can also be seen that the pit position generated by the drilling tooth during cutting rock

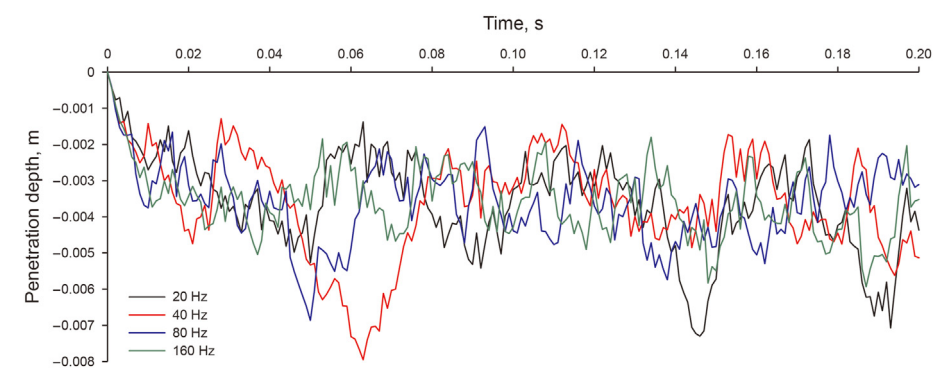


Fig. 38. Penetration depths under different impact frequencies.

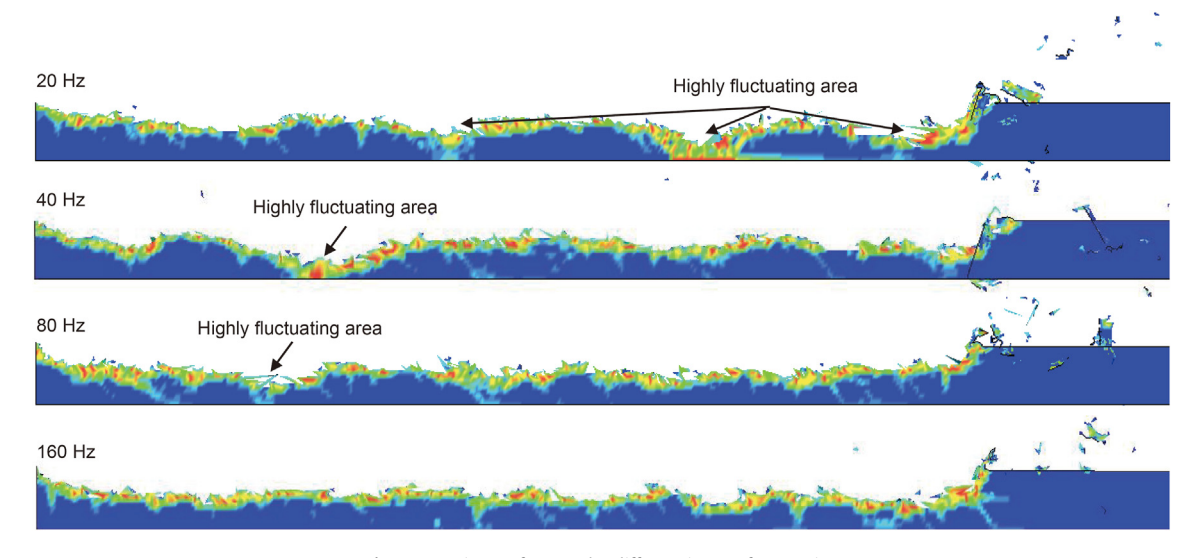
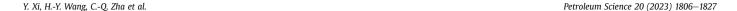


Fig. 39. Cutting surfaces under different impact frequencies.



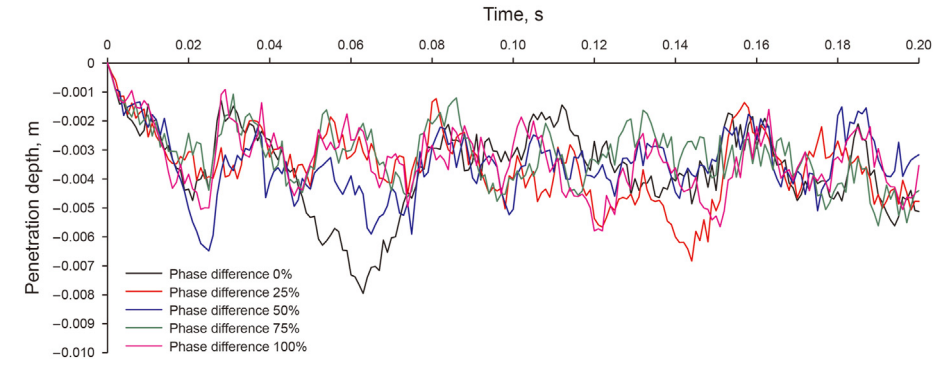


Fig. 40. Penetration depths under different phase transition conditions.

decreases with the increase of torsional impact load, which further shows that torsional impact has the effect of reducing stick-slip vibration.

As the torsional load increased, the diameter of the rock cuttings decreased (Fig. 30), thus retaining the cleanliness of the wellbore. This is related to the rock-breaking mechanism of the torsional impact load because a more significant circumferential load can break the rock more effectively.

(3) Axial and torsional impact amplitude changes

The amplitudes of the axial and torsional impact loads were changed to analyze their rock-breaking effects. The penetration depths for different torsional impact amplitudes are shown in Fig. 31. As the axial and torsional impact load amplitudes increased, the penetration depths also increased. The average penetration depths were 3.61 mm, 3.97 mm, and 4.35 mm, respectively.

According to the above analysis, the rock cuttings' size increased with the axial impact load and decreased with the increase in the torsional impact load. When the axial impact loads were equal, rock cuttings were more apparent, as shown in Fig. 32. When the increase in the torsional impact load was more significant than that of the axial impact load, the rock cuttings were small, such that the drilling speed increased and the wellbore cleanliness was retained.

5.2.3. Influence of impact frequency

(1) The torsional impact frequency remains unchanged and the axial impact frequency changes

The torsional impact frequency remained unchanged (40 Hz), while the axial impact frequencies (20 Hz, 40 Hz, 80 Hz, and 160 Hz) were changed. Fig. 33 shows the change in the penetration depth of the cutting teeth under different axial impact frequencies. It can be seen that when the axial frequency is less than 40 Hz, the amplitude fluctuation of the penetration depth is apparent. This fluctuation decreased as the axial frequency increased. The average penetration depths are 3.76 mm, 3.61 mm, 3.23 mm, and 3.37 mm in ascending order of frequency (Fig. 34). This is mainly because the attenuation of the stress waves in the rock accelerated with the increase in the impact frequency, leading to a decrease in the rock penetration depth (Zha et al., 2017).

Fig. 35 shows the debris under different axial impact frequencies. It can be seen that as the axial impact frequency increased, the size of the rock cuttings decreased, retaining the cleanliness of the wellbore.

(2) The axial impact frequency remains unchanged and the torsional impact frequency changes

The frequency of the axial impact load remained constant, while the frequency of the torsional impact changed. Fig. 36 shows the change in the penetration depth of the cutting teeth under different torsional impact frequencies. As the torsional impact frequency increased, the average penetration depths were 3.67 mm, 3.67 mm, 3.58 mm, and 3.38 mm (Fig. 37). It should be noted that when the torsional impact frequency was low, the drill teeth exhibited an apparent vibration. With the continuous increase in the torsional impact frequency, the vibration of the drill teeth gradually decreased.

(3) The axial and torsional impact frequency changes

The frequencies of the axial and torsional impact loads were changed simultaneously, and the change in the penetration depths under different frequency conditions was analyzed, as shown in Fig. 38. As the frequency increased, the penetration depth fluctuations decreased. The average penetration depths are 3.57 mm, 3.61 mm, 3.59 mm, and 3.56 mm at 20 Hz, 40 Hz, 80 Hz, and 160 Hz, respectively. It can be observed that changing the rock-breaking frequency had little effect on the penetration depth. As the frequency increased, the cutting surface became increasingly smooth, and the coverage area and the number of fluctuation areas decreased (Fig. 39).

5.2.4. Influence of phase difference

The phases of the axial and torsional shock waves can be adjusted by changing the structure of the coupled impact drill. As shown in Fig. 38, the phase differences between the axial and torsional shocks are 0%, 25%, 50%, 75%, and 100%. Fig. 40 shows the penetration depths of the drill teeth for different phase differences. As the phase difference increased from small to large, the average penetration depths were 3.61 mm, 3.55 mm, 3.48 m, 3.17 mm, and 3.34 mm, respectively (Fig. 41). It can be observed from the figure that the optimal effect was achieved with a phase difference of 0%. When the axial and torsional loads acted on the hard rock simultaneously, the penetration depth was the deepest. However, tripping occurred under these conditions. The penetration depth slightly decreased when the phase difference was 25%, but the vibration phenomenon was alleviated.

6. Conclusions

The motion mechanism of the axial-torsional coupled impact drilling tool and the dynamic rock characteristics during the impact

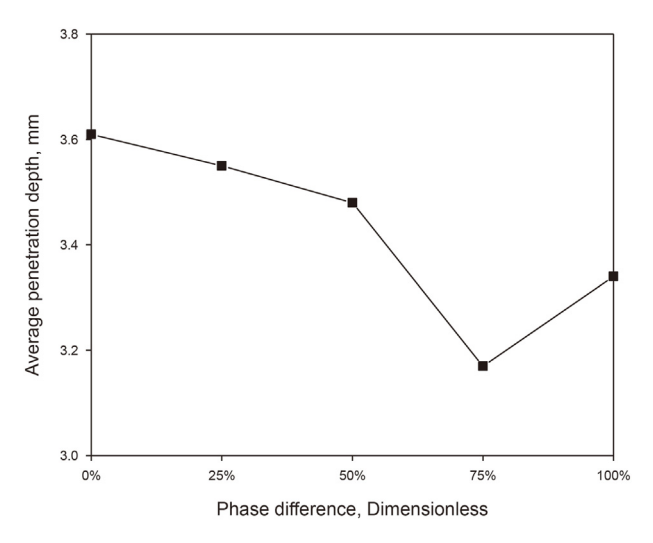


Fig. 41. Average penetration depths under different phase transition conditions.

rock-breaking process were examined. A numerical model of the PDC drill teeth during the rock-breaking process was established, and the stress wave parameters' influence on the drill teeth' penetration depth was studied. The conclusions are as follows.

- (1) Based on the laboratory test and numerical simulation of the SHPB, the relationship between the geometric and motion parameters of the impact hammer and the shock wave parameters was established. The cylindrical and spindle waveforms were in the shape of rectangular and sine waves, respectively. Increasing the wave velocity and hammer weight increased the impact amplitude. Increasing the hammer length increased the wavelength.
- (2) A numerical model of a PDC cutter and hard rock was established considering the RHT rock dynamic material model. The test results of a physical model verified the numerical simulation results. Compared with conventional drilling, the penetration depths of axial, torsional, and axialtorsional coupled impact drilling increased by 31.3%, 5.6%, and 34.7%, respectively.
- (3) Increasing the wavelength improved the penetration depth, indicating that an impact drilling tool with a long hammer should be selected for the vertical section. As the axial and torsional impact amplitudes increased, the penetration depths also increased. The size of the cuttings also decreased, retaining the cleanliness of the wellbore.
- (4) Increasing the axial or torsional impact frequency alone did not increase the penetration depth. This is because the increase in impact frequency accelerated the attenuation of the stress waves in the rock. Increasing the frequency in both directions had little impact on the penetration depth. However, increasing the frequency increased the smoothness of the cutting surface, which reduced the occurrence of bit vibrations.
- (5) When the impact frequency was 40 Hz, the penetration depth was the deepest with a phase difference of 0%, that is, the axial and torsional loads simultaneously acted on the hard rock. When the phase difference was 25%, the penetration depth decreased slightly, while the vibration was alleviated.

Declaration of competing interest

The authors declare that they have no known competing financial interests or personal relationships that could have appeared to influence the work reported in this paper.

Acknowledgments

This research was financially supported by the National Natural Science Foundation of China (52004013, U1762211).

References

- Baranowski, P., Kucewicz, M., Gieleta, R., et al., 2020. Fracture and fragmentation of dolomite rock using the JH-2 constitutive model: parameter determination, experiments and simulations. Int. J. Impact Eng. 140, 103543. https://doi.org/10.1016/j.ijimpeng.2020.103543.
- Cheng, Z., Sheng, M., Li, G.S., et al., 2019. Cracks imaging in linear cutting tests with a PDC cutter: characteristics and development sequence of cracks in the rock. J. Petrol. Sci. Eng. 179, 1151–1158. https://doi.org/10.1016/j.petrol.2019.04.053.
- Fan, L.F., Gao, J.W., Wu, Z.J., et al., 2018. An investigation of thermal effects on micro-properties of granite by X-ray CT technique. Appl. Therm. Eng. 140, 505–519. https://doi.org/10.1016/j.applthermaleng.2018.05.074.
- Fan, L.F., Wu, Z.J., Wan, Z., et al., 2017. Experimental investigation of thermal effects on dynamic behavior of granite. Appl. Therm. Eng. 125, 94–103. https://doi.org/ 10.1016/j.applthermaleng.2017.07.007.
- Franca, L.F.P., 2011. A bit-rock interaction model for rotary-percussive drilling. Int. J. Rock Mech. Min. Sci. 48 (5), 827–835. https://doi.org/10.1016/j.ijrmms.2011.05.007.
- Ji, Z.S., Shi, H.Z., Li, G.S., et al., 2020. Improved drifting oscillator model for dynamical bit-rock interaction in percussive drilling under high-temperature condition. J. Petrol. Sci. Eng. 186, 106772. https://doi.org/10.1016/ j.petrol.2019.106772.
- Li, B.D., Abdulwahab, A., Guo, D.Z., et al., 2020. ROP enhancement in high mud weight applications using rotary percussion drilling. In: Abu Dhabi International Petroleum Exhibition & Conference, 9–12 November, Abu Dhabi, UAE. https://doi.org/10.2118/203201-MS.
- Li, D.W., Wang, Y.X., 2015. Major issues of research and development of hot dry rock geothermal energy. Earth Sci. 40 (11), 1858–1869 (in Chinese).
- Li, X.B., Zhou, Z.L., Liu, D.S., et al., 2011. Wave Shaping by Special Shaped Striker in SHPB Tests. Advances in Rock Dynamics and Applications. CRC Taylor and Francis Press, New York.
- Li, Y.M., Zhang, T., Tian, Z.F., et al., 2021. Simulation on compound percussive drilling: estimation based on multi-dimensional impact cutting with a single cutter. Energy Rep. 7, 3833–3843. https://doi.org/10.1016/j.egyr.2021.06.057.
- Liao, M.L., Marian, W., Mukthar, S., et al., 2021. Experimental verification of the percussive drilling model. Mech. Syst. Signal Process. 146, 107067. https:// doi.org/10.1016/j.ymssp.2020.107067.
- Liu, G.H., Zha, C.Q., Li, J., et al., 2016. New technology with composite percussion drilling and rock breaking. Petroleum Drilling Techniques 44 (5), 5–15 (in Chinese).
- Liu, S.B., Ni, H.J., Wang, X.Y., et al., 2018. Rock-breaking mechanism study of axial and torsional impact hammer and its application in deep wells. In: IADC/SPE Asia Pacific Drilling Technology Conference and Exhibition, 27–29 August, Bangkok, Thailand. https://doi.org/10.2118/191077-MS.
- Liu, W., Qian, X., Li, T., et al., 2019. Investigation of the tool-rock interaction using Drucker-Prager failure criterion. J. Petrol. Sci. Eng. 173, 269–278. https://doi.org/10.1016/j.petrol.2018.09.064.
- Liu, W.J., Zeng, Y.J., Zhu, X.H., et al., 2020. Mechanism of rock breaking under composite and torsional impact cutting. Journal of China University of Petroleum (Edition of Natural Science) 44 (3), 74–80 (in Chinese).
- Mu, Z.J., Li, G.S., Huang, Z.W., et al., 2020. Status and development trend of vibration-impact ROP improvement technologies. Oil Drilling & Production Technology 42 (3), 253–260 (in Chinese).
- Shi, H., Li, G., Guo, B., et al., 2015. Hydraulic pulse jet: test of characteristics and field applications in ultra-deep wells. J. Nat. Gas Sci. Eng. 27, 200–206. https://doi.org/10.1016/j.ingse.2015.08.053.
- Singh, T.N., Jain, A., Sarkar, K., 2009. Petrophysical parameters affecting the microbit drillability of rock. Int. J. Min. Miner. Eng. 1 (3), 261–277. https://doi.org/10.1504/IJMME.2009.027256.
- Saksala, T., Gomon, D., Hokka, M., et al., 2014. Numerical and experimental study of percussive drilling with a triple-button bit on Kuru granite. Int. J. Impact Eng. 72, 56–66. https://doi.org/10.1016/ji.jijmpeng.2014.05.006.
- Staysko, R., Francis, B., Cote, B., 2011. Fluid hammer drives down well costs. In: SPE/IADC Drilling Conference and Exhibition, 1–3 March, Amsterdam, The Netherlands. https://doi.org/10.2118/139926-MS.

- Song, H.Y., Shi, H.Z., Zhao, S.J., et al., 2019. The percussive process and energy transfer efficiency of percussive drilling with consideration of rock damage. Int. J. Rock Mech. Min. Sci. 119, 1–12. https://doi.org/10.1016/j.ijrmms.2019.04.012.
- Song, H.Y., Shi, H.Z., Li, G.S., et al., 2021. Numerical simulation of the energy transfer efficiency and rock damage in axial-torsional coupled percussive drilling. J. Petrol. Sci. Eng. 196, 107675. https://doi.org/10.1016/j.petrol.2020.107675.
- Wang, P., Ni, H.J., Wang, R.H., 2018. A novel vibration drilling tool used for reducing friction and improve the penetration rate of petroleum drilling. J. Petrol. Sci. Eng. 165, 436–443. https://doi.org/10.1016/j.petrol.2018.02.053.
 Wang, W., Liu, G.H., Li, J., et al., 2021. Numerical simulation study on rock-breaking
- Wang, W., Liu, G.H., Li, J., et al., 2021. Numerical simulation study on rock-breaking process and mechanism of compound impact drilling. Energy Rep. 7, 3137—3148. https://doi.org/10.1016/j.egyr.2021.05.040.
- Wu, K., Ye, Z., 2019. The numerical research on rock breaking and rising mechanism of rotary-percussive drilling. Arabian J. Sci. Eng. 44 (12), 10561–10580. https:// doi.org/10.1007/s13369-019-04170-5.
- Xi, Y., Wang, W., Fan, L.F., et al., 2021. Experimental and numerical investigations on rock-breaking mechanism of rotary percussion drilling with a single PDC cutter. J. Petrol. Sci. Eng. 208, 109227. https://doi.org/10.1016/j.petrol.2021.109227.
- Xi, Y., Wang, W., Zha, C.Q., et al., 2022. Numerical investigations on rock breaking

- mechanism and parameter influence of torsional percussive drilling with a single PDC cutter. J. Petrol. Sci. Eng. 210, 110077. https://doi.org/10.1016/i.petrol.2021.110077.
- Xu, Z.C., Jin, Y., Hou, B., et al., 2016. Rock breaking model under dynamic load with the application of torsional and axial percussion hammer. In: International Petroleum Technology Conference, 14–16 November, Bangkok, Thailand. https://doi.org/10.2523/IPTC-18777-MS.
- Zha, C.Q., Liu, G.H., Li, J., et al., 2017. The rock breaking mechanism of the compound percussive-rotary drilling method with a PDC bit. Petroleum Drilling Techniques 45 (2), 20–24 (in Chinese).
- Zhang, X., Zhang, S., Luo, Y., et al., 2019. Experimental study and analysis on a fluidic hammer-an innovative rotary-percussion drilling tool. J. Petrol. Sci. Eng. 173, 362—370. https://doi.org/10.1016/j.petrol.2018.10.020.
 Zhang, Z.Z., Zhao, D.J., Zhao, Y., et al., 2020. Simulation and experimental study on
- Zhang, Z.Z., Zhao, D.J., Zhao, Y., et al., 2020. Simulation and experimental study on temperature and stress field of full-sized PDC bits in rock breaking process. J. Petrol. Sci. Eng. 186, 106679. https://doi.org/10.1016/j.petrol.2019.106679.
- Zhang, Z.Z., Zhao, D.J., Zhao, Y., et al., 2021. 3D numerical simulation study of rock breaking of the wavy PDC cutter and field verification. J. Petrol. Sci. Eng. 203, 108578. https://doi.org/10.1016/j.petrol.2021.108578.